6-1980

# Chemical Trends in the Ice Springs Basalt, Black Rock Desert, Utah

W. C. Lynch
*Department of Geology and Geophysics, University of Utah*

W. P. Nash
*Department of Geology and Geophysics, University of Utah*

DOE/ID/12079-12



TOPICAL REPORT

# CHEMICAL TRENDS IN THE ICE SPRINGS BASALT, BLACK ROCK DESERT, UTAH

By

**W. C. Lynch and W. P. Nash**

*Work performed under Contract No.*

**DE-AC07-80ID12079**

***Department of Geology and Geophysics***

***University of Utah***

***Salt Lake City, Utah (USA)***

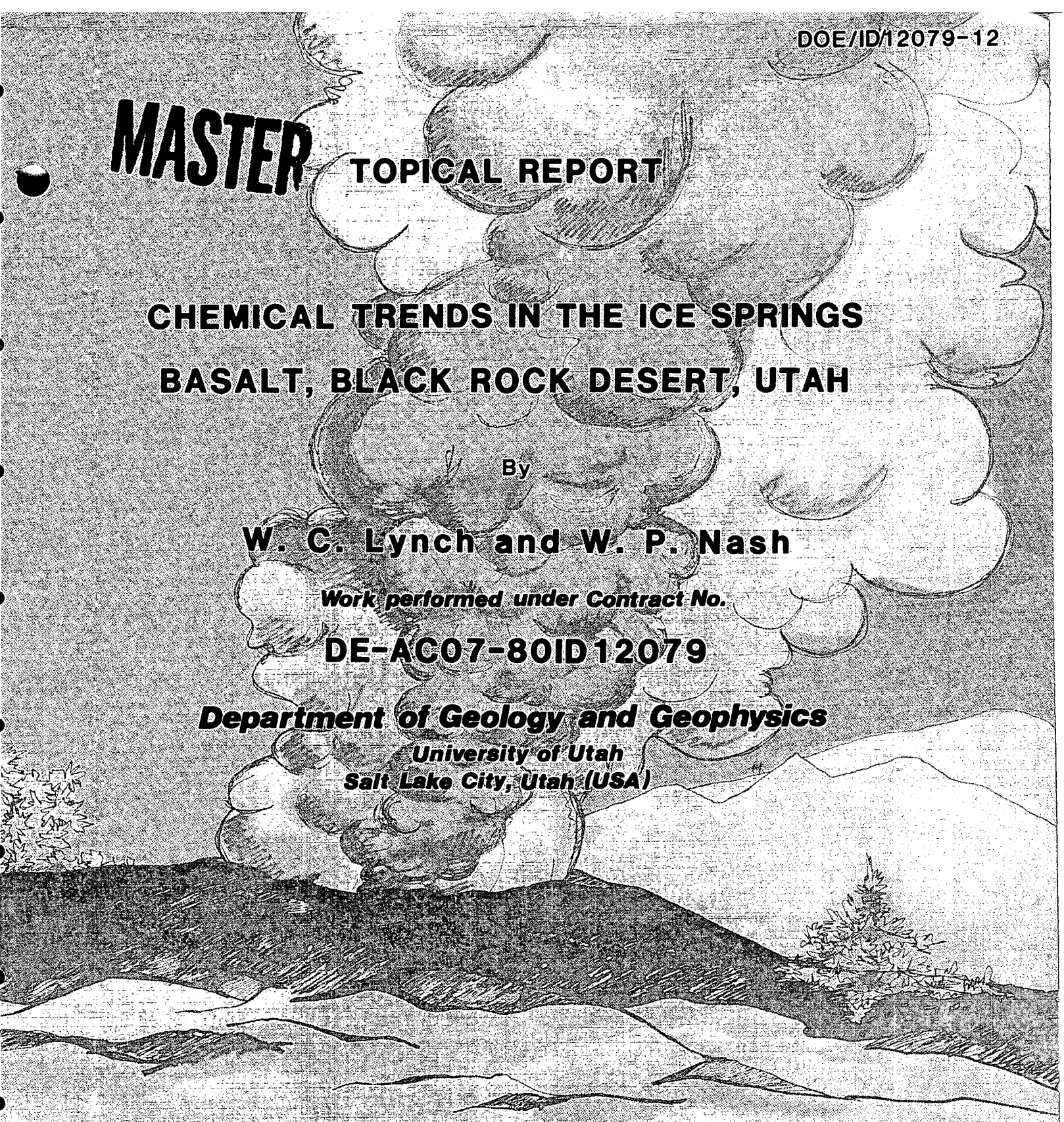

**June 1980**

***Prepared for***

***DEPARTMENT OF ENERGY***

***Division of Geothermal Energy***

## DISCLAIMER

## NOTICE

This report was prepared to document work sponsored by the United States Government. Neither the United States nor its agent, the United States Department of Energy, nor any Federal employees, nor any of their contractors, subcontractors or their employees, makes any warranty, express or implied, or assumes any legal liability or responsibility for the accuracy, completeness, or usefulness of any information, apparatus, product or process disclosed, or represents that its use would not infringe privately owned rights.

## NOTICE

Reference to a company or product name does not imply approval or recommendation of the product by the University of Utah or the U.S. Department of Energy to the exclusion of others that may be suitable.

DOE/ID12079-12

# CHEMICAL TRENDS IN THE ICE SPRINGS BASALT, BLACK ROCK DESERT, UTAH

by

W. C. Lynch and W. P. Nash

## ABSTRACT

The Holocene Ice Springs volcanic field of west-central Utah consists of 0.53 $km^3$ of tholeiitic basalts erupted as a sequence of nested cinder cones and associated lava flows. Whole rock X-ray fluorescence and atomic absorption analysis of ninety-six samples of known relative age document statistically significant inter- and intra-eruption chemical variations. Elemental trends include increases in Ti, Fe, Ca, P, and Sr and decreases in Si, K, Rb, Ni, Cr, and Zr with decreasing age. Microprobe analyses of microphenocrysts of olivine, plagioclase, and Fe-Ti oxides and of groundmass olivine, plagioclase, and clinopyroxene indicate limited chemical variation between mineral assemblages of the eruptive events. Petrographic analyses have identified the presence of minor amounts of silicic xenoliths, orthopyroxene megacrysts, and plagioclase xenocrysts. Potassium-argon determinations establish the existence of excess argon in the basaltic cinder ($30.05 \times 10^{-12}$ moles/gm) and in distal lava flows ($8.29 \times 10^{-12}$ moles/gm) which suggest apparent "ages" of 16 and 4.3 million years respectively. Strontium isotopic data (Puskar and Condie, 1973) show systematic variations from oldest eruptions ($^{87}Sr/^{86}Sr=0.7052$) to youngest eruptions ($^{87}Sr/^{86}Sr=0.7059$).

Theoretical evaluation of observed major element, trace element, isotopic, and thermophysical properties of the lavas and cinders limits the importance of proposed magmatic differentation processes. The data

are compatible with a model involving crystal fractionation, crustal assimilation, and magma mixing. Initial modification of mantle derived melts resulted from olivine fractionation at depth. Subsequent combination of 6 to 8% fractionation of plagioclase, minor olivine, and magnetite at shallow depths, less than one percent assimilation of silicic crustal basement rocks, and interaction of compositionally similar magma pulses explains the overall inter-eruption chemical trends. The intra-eruption variations follow the overall trends and a similar combination of processes of lesser magnitude accounts for the intra-eruption variations.

TABLE OF CONTENTS

LIST OF FIGURES

## LIST OF TABLES



## LIST OF APPENDICES

## ACKNOWLEDGMENTS

Financial support was provided by a grant from the University of Utah's Geology Special Funds and from the Department of Energy, Division of Geothermal Energy, Contract number DE-AC07-80ID12079.

We particularly appreciate the assistance of Drs. S. H. Evans, Jr. and F. H. Brown. They provided the argon analyses and lively discussions.

# INTRODUCTION

The relative importance of various processes of magmatic differentiation may be evaluated through the interpretation of systematic chemical variations in sequential eruptions of volcanic rocks. The Holocene Ice Springs volcanic field, located in the Black Rock Desert of west-central Utah, affords an excellent opportunity to study several scales of chemical variation in continental tholeiitic basalts. Initial descriptions of the Ice Springs basalts were made by Gilbert (1890). He presented an accurate and thorough description of many Ice Springs volcanic features and his preliminary observations on the sequence of eruptions remain valid today. Condie and Barsky (1972) and Puskar and Condie (1973) presented results of a regional petrological analysis of the Black Rock Desert volcanics. In their work, they identified regional long-term chemical variations within the Black Rock Desert and localized short-term time dependent chemical variations within the Ice Springs field. They considered the long-term trends to represent fundamental changes in magmatic differentiation processes during the lifetime of the volcanic province; whereas, the short-term trends represented changes in local differentiation processes during the eruptive events of the Ice Springs field. The long-term regional variations included a decrease in Sr and systematic increase in K, Rb, and 87Sr/86Sr from oldest to youngest. The short-term "Ice Springs" trend included increases in Fe, Mn, Sr, and

$^{87}Sr/^{86}Sr$ with decreases in Si, Mg, Na, K, Rb, and Ni from early to late. They attributed the chemical variation to long-term effects of crystal fractionation, crustal assimilation, and possible mixing of residual differentiated magmas. Subsequent work by Hoover (1974) supported the earlier observations of short-term and long-term chemical trends in the Black Rock Desert and Ice Springs basalts.

## FIELD RELATIONS

The Ice Springs volcanic field consists of a series of nested cinder cones and related lava flows. Based on the preliminary observations of Gilbert (1890), Hoover (1974) outlined the Ice Springs eruptive sequence as initial eruptions and flows northward followed by westward flows and culminated by flows southeastward. Associated with the flows, Hoover (1974) identified the sequence of formation of four major cinder-spatter cones. The largest, the Crescent, served as the source vent for the northern flows. The second largest, the Miter, developed on the southwestern rim of the earlier Crescent and was the source vent for the southwestward flows. A third large cone, the Terrace, was built onto the southern side of the Miter-Crescent cone and served as the source vent for the final southeastward flows. Hoover (1974) named a fourth cone, the Pocket, located within the outline of the earlier formed Crescent. The Pocket is a symmetrical cinder-spatter cone which produced only a small amount of lava. Each of the cinder cones display breached rims where lavas have flowed outward. The western half of the Crescent cone has been completely destroyed by subsequent flows and by the development of the Miter and Pocket cones. The Miter cone has been breached on the southwest and north sides. The lava channel from the northern side of the Miter is deflected by the Pocket cone, but at the same time, these Miter flows truncate lavas flowing out of a breach in the western side of the

Pocket cone. The Terrace cone has been breached on the southwest and southeast sides. The lava channel from the southwest breach of the Miter deflects flows from the southwestern breach of the Terrace. These cross-cutting relations indicate an eruptive sequence of initial Crescent cinders and flows northward followed by early Miter cinder and flows westward, followed by concurrent Pocket and Miter cinder and flows northward, and eruption terminated with Terrace cinders and flows to the southeast and southeastward.

The flow character of the lavas changes noticeably from proximal slabby pahoehoe to distal aa. The slabby pahoehoe predominates in the well defined lava channels near the source vents. The pahoehoe texture appears to develop as underlying lava is drained out to feed the advancing lava front (Williams and McBirney, 1979). The transition to blocky aa clinker and rubble is abrupt at the channel margins, but in distal portions of the flows confusing rubble-clinker pile-ups make interflow identification difficult. The major flow lobes -- northern, southwestern, and southeastern were found to be related to the major cinder vents -- Crescent, Miter, and Terrace respectively. Subdivision of the lobes into smaller units was possible only where well defined rubble fronts enable distinction of flows to be made. Figure 1 shows the approximate surface expressions of the major flow units and the location of the cinder cones.

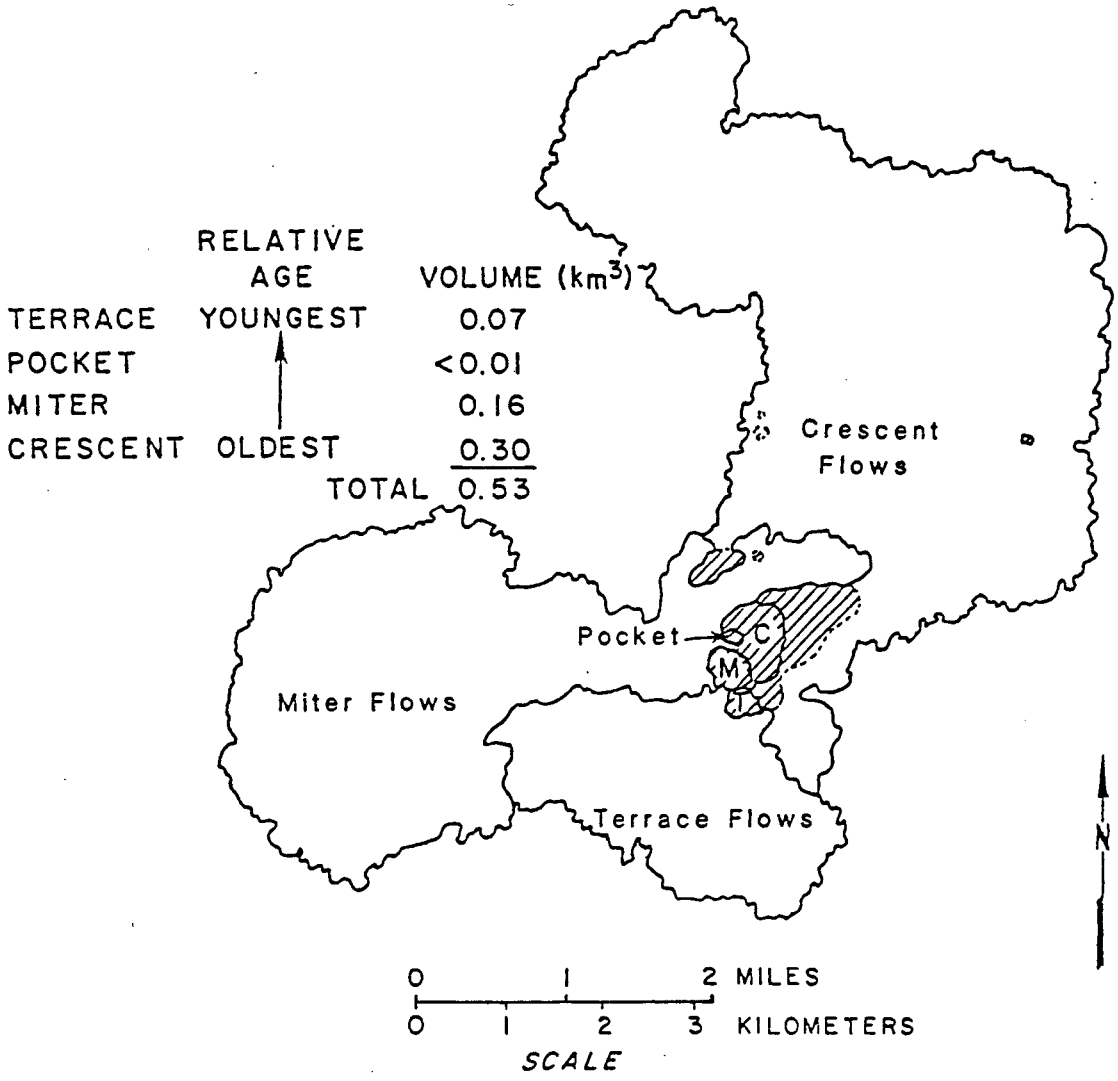


Figure 1. Generalized map showing distribution of lava and cinder in the Ice Springs volcanic field.

## SAMPLE COLLECTION AND ANALYTICAL TECHNIQUES

Recent large scale mining of the Ice Springs cinder cones has exposed the detailed internal structures of all the major cinder cones. This exposure enables the systematic sampling of the intra-eruption variations as well as the inter-eruption variations from cone to cone and flow to flow. To determine the chemical variation within an individual cinder cone, 200 gram samples were collected at approximately 1 meter intervals through the exposed sections of the four major cones. Care was taken to avoid sampling fragments of silicious inclusions, and all samples were the cleanest and least oxidized at the particular horizon. For the Crescent, 30 samples were collected on a 30 meter traverse from the top of the cone's east side down the outer east slope. For the Terrace, 20 samples were collected on a 25 meter traverse from the northeastern corner of the cone down the inner slope. For the miter, 13 samples were collected along a 30 meter traverse for the top of the cone's southeast side down the inner slope. And, for the Pocket, 9 samples were collected along a 15 meter traverse from the upper northwestern edge of the cone down the exposed outer western slope. 2 kilogram samples of lava were collected along and within the various flow units to characterize the lavas asspciated with the cinder cones. Representative samples of lava within each of the cinder cones were also sampled. Care was taken to collect clean lava samples and to avoid samples contaminated with carbonate or

aerially transported gypsiferous dust.

Whole rock sample preparations involved washing each sample in distilled water to remove any dirt or dust comtaminates and then drying the sample at 100°C overnight. Once dry, the samples were hand picked to remove excessively carbonate contaminated fragments and fragments of silicious inclusions. The selected materal was crushed in a tungsten-carbide jaw crusher and then powdered in a tungsten-carbide shatter box. Whole rock major and trace element analyses were performed by standard X-ray fluorescence techniques (Norrish and Hutton, 1969) using USGS standards (Flanagan, 1972) and University of Utah internal standards BRD 77-12 and SBV 76-23 (Nash and Crecraft, 1979; Evans and Nash, 1979). In addition, Ni and Cr were analyzed by atomic absorbtion techniques. Total iron was analyzed as $Fe_2O_3$ and the relative abundances of FeO to $Fe_2O_3$ were calculated on the basis of BRD 77-12 as 6.86. Loss was measured as weight lost on ignition at 1000°C for 40 minutes.

In order to determine analytical error, 10 replicate major element analyses and 5 trace element analyses were performed on the University of Utah standard BRD 77-12, an Ice Spring basalt. The average values and the associated standard deviations are listed along with the wet chemical standard determinations in Table 1. When these values are compared to the averages and standard deviations for the Ice Springs cinders and flows, significant variations beyond analytical error are seen to exist in all elements except Nb and Th.

Table 1. Whole Rock Analytical Error Analysis as Average and Standard Deviation. Oxidation Ratio for All Ice Springs Values Same As BRD 77-12 Wet Chemical Analysis.

| | BRD 77-12 XRF(N=10) | | BRD 77-12 Wet Chemical | All Ice Springs XRF(N=85) | |
|---|---|---|---|---|---|
| wt% | mean | std.dev. | mean | mean | std.dev. |
| $SiO_2$ | 49.45 | .57 | 48.99 | 50.88 | 1.29 |
| $TiO_2$ | 1.93 | .03 | 2.04 | 1.79 | .18 |
| $Al_2O_3$ | 15.48 | .17 | 14.99 | 15.40 | .35 |
| $Fe_2O_3$ | 1.39 | .04 | 1.39 | 1.27 | .08 |
| FeO | 9.56 | .27 | 9.53 | 8.85 | .59 |
| MnO | .19 | .01 | .19 | .18 | .01 |
| MgO | 7.74 | .14 | 7.83 | 7.33 | .42 |
| CaO | 9.95 | .14 | 9.67 | 8.86 | .31 |
| $Na_2O$ | 2.80 | .18 | 2.81 | 2.85 | .30 |
| $K_2O$ | .99 | .01 | .99 | 1.27 | .16 |
| $P_2O_5$ | .56 | .02 | .61 | .53 | .06 |
| Loss | .37 | - | .37 | .41 | .40 |
| Total | 100.41 | - | 99.41 | 99.62 | - |
| | XRF(N=5) | | Standard XRF | XRF(N=85) | |
| Nb* | 17 | 1.1 | 25 | 20 | 1.9 |
| Zr* | 142 | 5.3 | 182 | 159 | 11 |
| Y* | 28 | 2.7 | 45 | 29 | 1.8 |
| Sr* | 360 | 4.9 | 428 | 358 | 15.6 |
| Rb* | 20 | 3.4 | 18 | 25 | 4.9 |
| Th* | 7 | 3.0 | 5 | 5 | 3.2 |
| Ni* | 149 | 2.0 | 149 | 128 | 12.6 |
| Cr* | 235 | 9.0 | 235 | 227 | 30.0 |

*parts per million.

## PETROGRAPHY AND MINERALOGY

The lavas of the Ice Springs volcanic field display little systematic petrographic variation. Table 2 summarizes the average modal abundances for the four major Ice Springs eruptive units. The basalts are typically very fine grained with a microporphyritic to weakly glomeroporphyritic, intersertal to intergranular texture. The microphenocrysts constitute less than 8% of the rocks and consist of olivine, plagioclase, and Fe-Ti oxides. The groundmass constitutes the bulk of the rocks and consists of very fine grained intersertal to intergranular mixtures of anhedral clinopyroxene, lath shaped plagioclase, granular olivine, granular opaques, needle shaped apatite, and brown glass. Vesicles are abundant in several samples, and the void spaces were normalized out of the modal analyses to allow for comparison of the eruptive units. Two important petrographic features of the basalts include the presence of minor amounts of orthopyroxene megacrysts with olivine reaction rims and silicious inclusions with resorbtion-assimilation rims.

### Olivine

The olivine microphenocrysts display two distinct morphologies. These include subequant to euhedral internally skeletal crystals and elongate hollow skeletal crystals .2 to .4 mm in diameter. The compositional variation of the groundmass and microphenocryst olivine between and within the eruptive units is shown in Figure 2 and average

Table 2. Modal analyses of Ice Springs basalts (volume percent)

| | Crescent | Miter | Pocket | Terrace |
|---|---|---|---|---|
| Olivine | 4-6 | 4-6 | 4-5 | 4-6 |
| Plagioclase | 1-2 | 1-2 | 1 | 2-3 |
| Fe-Ti Oxides | 2-3 | 2-3 | 1-2 | 1-2 |
| Groundmass | 88-92 | 88-92 | 92-94 | 88-90 |
| Assimilated Xenoliths | .5 | .7 | .5 | .6 |
| OPX megacrysts | yes | yes | no | no |

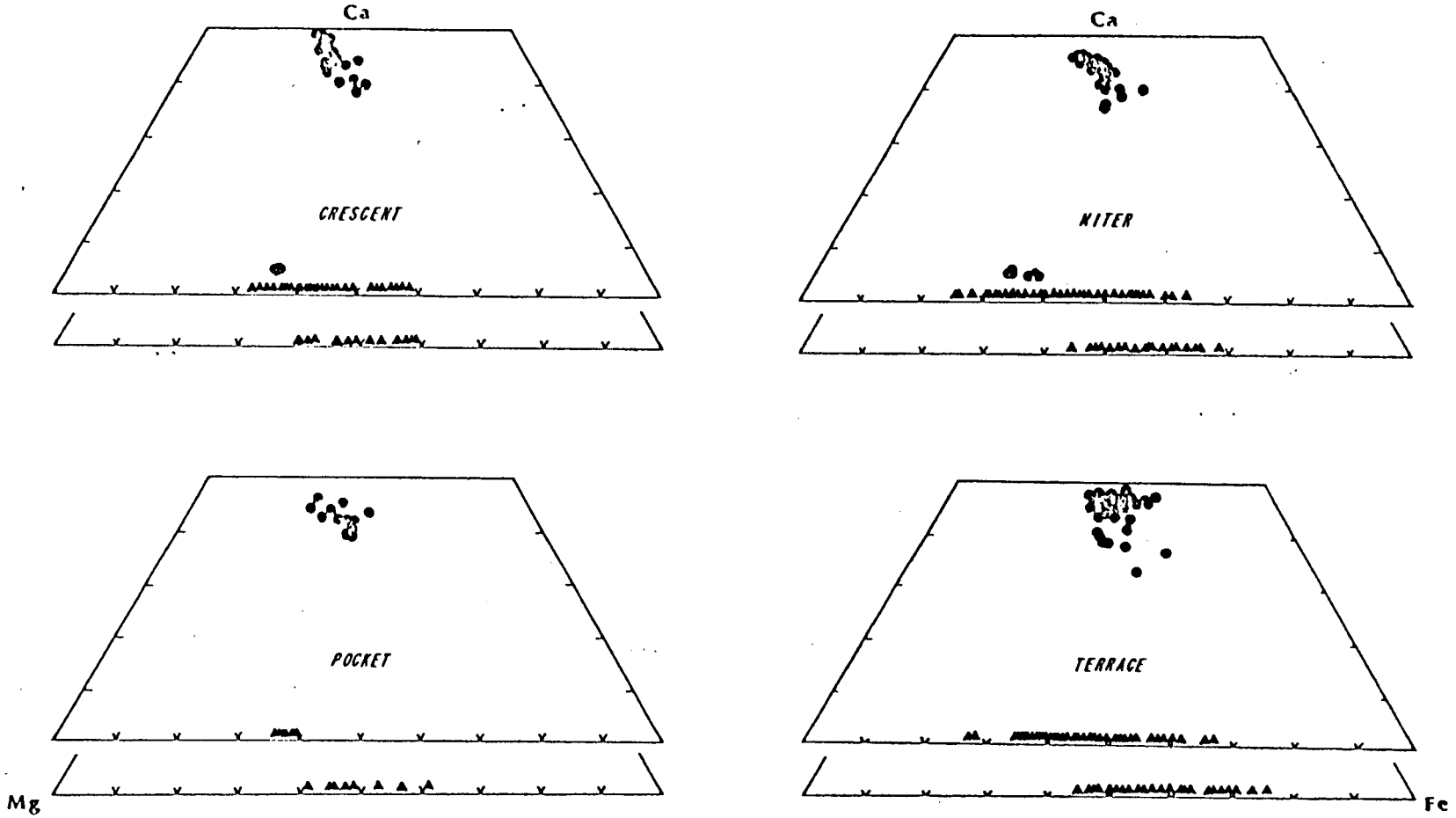


Figure 2. Microprobe analyses of groundmass, phenocryst, and megacryst pyroxenes and olivines plotted in terms of atom percent Mg, Fe, Ca. Filled circles are pyroxenes and triangles are olivines. Groundmass olivines are in lower diagram in set.

analyses are listed in Table 3. The phenocrysts generally show limited compositional variation between the eruptive sequences and each sequence shows overlapping zoning from $Fo_{88}$ to $Fo_{60}$. The lack of variation in the phenocryst data suggests a consistent and limited crystallization interval for the phenocryst phases. The groundmass olivine in all eruptive units tends towards depletion in magnesium compared to the associated phenocrysts and contrary to the restricted variation between eruptive events for the phenocryst data, the groundmass olivine of the Terrace and Miter samples display trends of increasing iron content when compared to Crescent samples. No significant calcium zoning is observed in both the groundmass and phenocryst olivine. The chemistry and morphology of the olivine groundmass and phenocrysts suggest a two stage cooling history. Donaldson et al. (1975) experimentally produced similar morphologies in lunar basalt crystallization experiments. His results indicate that a slow pre-eruption crystallization stage will produce the subequant to euhedral skeletal crystals and that a rapid continuously increasing post-eruption crystallization stage will produce the elongate to euhedral hollow skeletal crystals. The weakly glomeroporphyritic texture suggests syneutic accretion in a turbulent preeruptive conduit (Vance, 1969).

Plagioclase

The plagioclase microphenocrysts are of two distinct types. The first are phenocrysts or xenocrysts .5 to 1 cm long, zoned, and partially resorbed. These large plagioclase crystals are found in

Table 3. Average microprobe analyses and structural formulas of olivines.

| | Phenocrysts | | | | Groundmass | | | |
|---|---|---|---|---|---|---|---|---|
| | ISB-42 | ISB-40 | ISB-80 | ISB-84 | ISB-42 | ISB-40 | ISB-80 | ISB-84 |
| $SiO_2$ | 38.32 | 38.49 | 38.92 | 37.88 | 37.97 | 37.32 | 37.92 | 35.44 |
| FeO | 21.70 | 18.98 | 21.92 | 24.27 | 30.37 | 26.84 | 29.33 | 39.94 |
| MnO | .56 | .34 | .40 | .47 | .60 | .53 | .54 | .78 |
| MgO | 38.27 | 40.28 | 38.86 | 36.63 | 30.90 | 33.38 | 32.03 | 23.22 |
| CaO | .62 | .60 | .60 | .61 | .68 | .73 | .64 | .72 |
| NiO | .14 | .18 | .13 | .12 | .09 | .10 | .11 | .10 |
| Total | 99.6 | 98.9 | 100.9 | 100.0 | 100.6 | 98.9 | 100.6 | 100.2 |
| | Number of atoms based on 4 oxygens | | | | | | | |
| Si | 1.00 | 1.00 | 1.00 | 1.00 | 1.02 | 1.00 | 1.01 | 1.01 |
| Fe | .47 | .41 | .47 | .54 | .68 | .61 | .66 | .95 |
| Mn | .01 | .01 | .01 | .01 | .01 | .01 | .01 | .02 |
| Mg | 1.49 | 1.56 | 1.49 | 1.44 | 1.24 | 1.34 | 1.28 | .99 |
| Ca | .02 | .02 | .02 | .02 | .02 | .02 | .02 | .02 |
| Ni | .00 | .00 | .00 | .00 | .00 | .00 | .00 | .00 |
| | 1.99 | 2.00 | 1.99 | 2.01 | 1.95 | 1.98 | 1.97 | 1.98 |

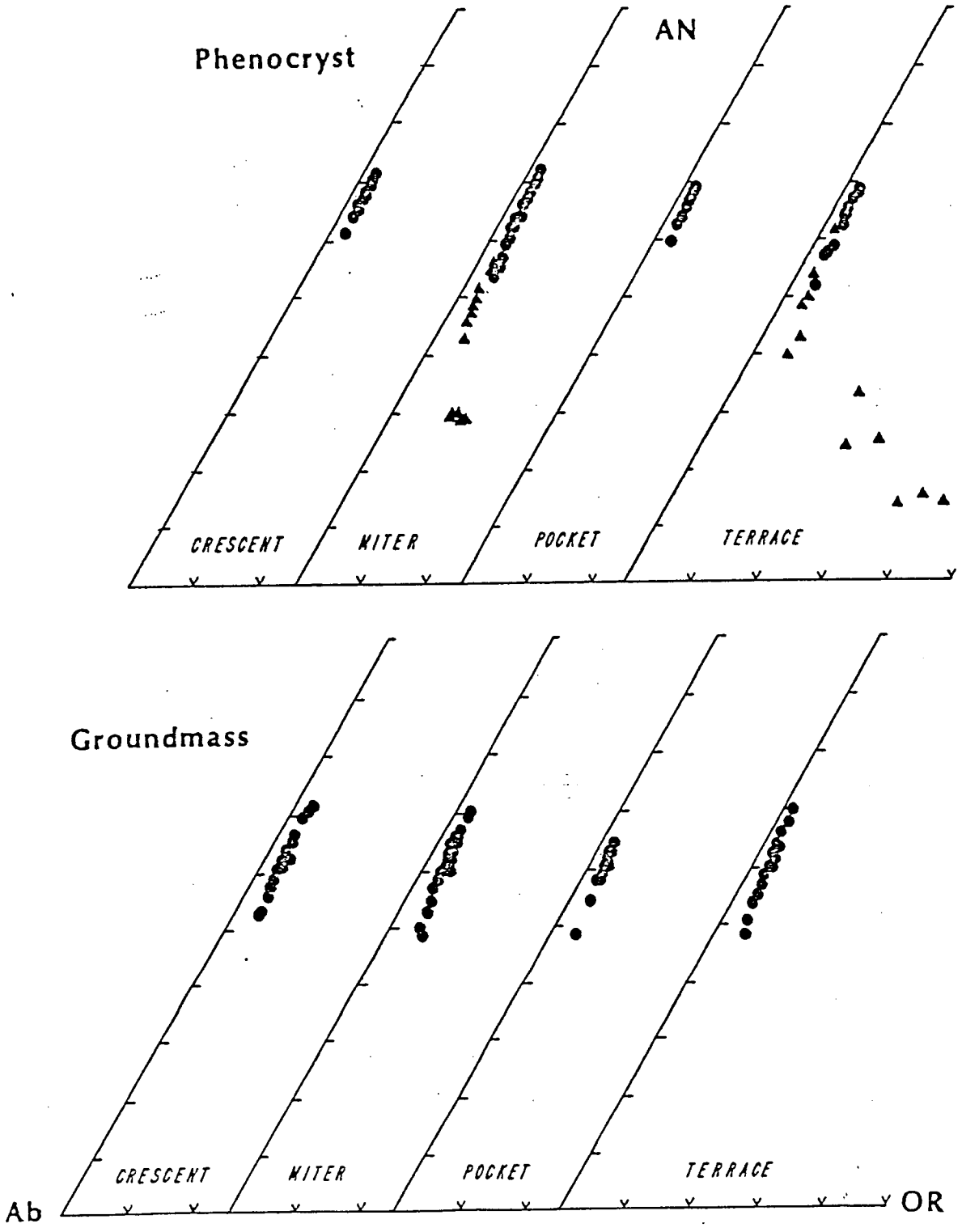


Figure 3. Microprobe analyses of groundmass, phenocryst, and xenocryst feldspars plotted in terms of mole percent AN, OR, and AB. Solid circles are phenocryst and triangles are xenocrysts. Groundmass is plotted in lower diagrams.

Table 4. Average microprobe analyses of feldspars

| | Phenocrysts | | | | Groundmass | | | | Xenolith |
|---|---|---|---|---|---|---|---|---|---|
| | ISB-42 | ISB-40 | ISB-80 | ISB-84 | ISB-42 | ISB-40 | ISB-80 | ISB-80 | ISB-42 |
| CaO | 13.37 | 13.32 | 12.92 | 12.65 | 12.64 | 12.62 | 12.12 | 12.97 | 6.03 |
| $K_2O$ | .37 | .32 | .32 | .35 | .50 | .36 | .49 | .33 | 1.80 |
| $Na_2O$ | 3.74 | 3.72 | 3.91 | 4.03 | 4.06 | 4.14 | 4.29 | 3.86 | 6.92 |
| BaO | .04 | .04 | .03 | .04 | .04 | .04 | .03 | .04 | .02 |
| SrO | .09 | .08 | .09 | .07 | .07 | .08 | .07 | .07 | .12 |
| FeO | 1.07 | .97 | .81 | .89 | 1.31 | 1.16 | .92 | 1.05 | .25 |
| Stoichio-metric Total | 100.2 | 99.5 | 99.1 | 98.9 | 100.0 | 99.8 | 99.4 | 98.9 | 99.1 |
| AN* | 64.97 | 65.19 | 63.34 | 62.13 | 61.41 | 61.44 | 59.22 | 63.74 | 29.14 |
| OR* | 2.14 | 1.86 | 1.87 | 2.05 | 2.89 | 2.09 | 2.85 | 1.93 | 10.36 |
| AB* | 32.89 | 32.95 | 34.72 | 35.82 | 35.69 | 36.47 | 37.93 | 34.33 | 60.51 |

* mole %

almost every sample but are volumetrically insignificant. The second type of microphenocryst is dominant and consists of euhedral, elongate, and unzoned microphenocrysts .2 to .4 mm long. Plagioclase is also abundant in the groundmass. As shown in Figure 3 and listed in Table 4, plagioclase groundmass and phenocryst compositions vary little in composition between the various flow units. The range in average composition for the Ice Springs basalts is generally from $An_{56}Ab_{42}Or_2$ to $An_{70}Ab_{28}Or_2$ for phenocrysts and $An_{50}Ab_{48}Or_2$ to $An_{61}Ab_{37}Or_2$ for groundmass. Alkali feldspars are lacking as a primary mineral phase in the basalts. However, the variable and alkalic nature of the xenocryst and inclusion feldspars is shown in Figure 3. Generally the xenocrysts of plagioclase are enriched in sodium and potassium and range in composition from $An_{50}Ab_{48}Or_2$ to $An_{30}Ab_{67}Or_3$. The alkali feldspars from some of the silicious inclusions undergoing assimilation have compositions averaging $An_{29}Ab_{60}Or_{11}$. The microporphyritic texture of the plagioclase is compatible with the two stage cooling model suggested by the olivine data. However, the large plagioclase xenocrysts and inclusions imply that some additional processes of fractionation or assimilation may have taken place.

Fe-Ti Oxides

The Fe-Ti oxides occur as microphenocrysts of euhedral to granular ilmenite and magnetite, .05 to .15 mm in diameter. Chromites are common as inclusions in olivine microphenocrysts, and some chromite occurs in the intersertal groundmass of the early Crescent flows. Table 5 gives the average analyses for ilmenites, magnetites, and

Table 5. Average microprobe analyses of Fe-Ti oxides and spinels.

| | Magnetites | | | Chromites | | Ilmenites | | |
|---|---|---|---|---|---|---|---|---|
| | ISB-42 | ISB-84 | ISB-41 | ISB-42 | ISB-70 | ISB-42 | ISB-84 | ISB-41 |
| $SiO_2$ | .95 | .52 | .65 | .87 | .56 | 1.08 | .54 | 1.68 |
| $TiO_2$ | 19.1 | 21.9 | 21.0 | 1.51 | 2.17 | 46.9 | 49.8 | 41.3 |
| $Al_2O_3$ | 2.19 | 2.49 | 1.73 | 28.41 | 26.61 | .42 | .32 | 1.87 |
| $Cr_2O_3$ | 1.00 | .91 | 1.57 | 28.22 | 28.33 | .31 | .05 | .04 |
| FeO | 71.5 | 68.0 | 71.1 | 30.0 | 33.0 | 46.4 | 46.2 | 53.7 |
| MgO | 3.27 | 2.11 | 2.03 | 10.53 | 8.01 | 4.07 | 1.96 | 2.07 |
| MnO | .58 | .56 | .72 | .23 | .33 | .52 | .58 | .76 |
| Sum | 98.6 | 96.5 | 98.8 | 99.7 | 99.0 | 99.7 | 99.4 | 101.4 |
| Recalc. | | | | | | | | |
| $Fe_2O_3$ | 29.1 | 21.9 | 24.2 | | | 11.9 | 5.4 | 21.1 |
| FeO | 45.3 | 48.3 | 49.3 | | | 35.7 | 41.3 | 34.7 |
| Total | 101.5 | 98.7 | 101.2 | | | 100.9 | 100.0 | 103.5 |
| Ulvosp.* | 54.8 | 62.8 | 59.1 | | | | | |
| $Fe_2O_3$* | | | | | | 11.8 | 5.6 | 22.2 |

* mole %

chromites from each of the flow units. Little significant variation exists between the flow units, and the variation in values reflect the uncertainty in analysis of the very fine grained oxides. Generally, the ulvospinel compositions range from 55 to 62 mole percent and hematite compositions range from 6 to 22 mole percent. The high hematite values likely represent post crystallization oxidation and exsolution. However, little textural evidence of oxidation and exsolution was observed optically.

Pyroxenes

Orthopyroxene occurs as large .5 to .3 cm unzoned megacrysts. The presence of the orthopyroxene megacryst phase is of significance because of its apparent disequilibrium with the host basalt. The disequilibrium is displayed as olivine reaction rims surrounding the homogeneous orthopyroxene crystals. Additional evidence for disequilibrium is the lack of orthopyroxene in the groundmass or phenocryst assemblage. Average analyses of groundmass clinopyroxene and megacryst orthopyroxene are given in Table 6. Figure 3 displays the variation in pyroxene analyses throughout the four eruptive units. Orthopyroxene was found only in the Miter and Crescent lavas and its composition is uniform between the two units. The clinopyroxene varies from a magnesium rich variety in the early Crescent to a more iron rich type in the later Miter and Terrace samples. The uniform composition of the orthopyroxene and its reaction relation with the host basalt indicates that the orthopyroxene is not in the low pressure equilibrium assemblage of the Ice Springs basalts.

Table 6. Average microprobe analyses and structural formulas of pyroxenes.

| | Megacrysts | | | | Groundmass | | | |
|---|---|---|---|---|---|---|---|---|
| | ISB-42 | ISB-90A | ISB-103 | ISB-103 | ISB-42 | ISB-40 | ISB-80 | ISB-84 |
| $SiO_2$ | 51.3 | 52.2 | 53.0 | 52.6 | 52.7 | 50.5 | 53.0 | 51.3 |
| $TiO_2$ | .23 | .26 | .21 | .20 | .80 | 1.80 | .95 | .21 |
| $Al_2O_3$ | 6.24 | 6.28 | 5.21 | 6.25 | 3.90 | 4.60 | 3.60 | 3.27 |
| $Cr_2O_3$ | .08 | .05 | .14 | n.a. | .04 | n.a. | n.a. | .23 |
| FeO | 11.1 | 12.7 | 12.2 | 8.1 | 10.4 | 11.2 | 8.9 | 10.6 |
| MnO | .32 | .30 | .27 | .28 | .30 | .37 | .34 | .37 |
| MgO | 28.6 | 26.5 | 27.5 | 16.7 | 14.4 | 12.8 | 15.5 | 13.8 |
| CaO | 2.18 | 1.98 | 1.90 | 17.56 | 17.15 | 18.84 | 18.14 | 18.42 |
| $Na_2O$ | .11 | .10 | .08 | .07 | .29 | .37 | .34 | .36 |
| NiO | .05 | .02 | .01 | .03 | .04 | .03 | .04 | .04 |
| Total | 100.2 | 100.5 | 100.5 | 101.9 | 100.0 | 100.5 | 100.8 | 99.6 |

Number of atoms based on 6 oxygens.

| | | | | | | | | |
|---|---|---|---|---|---|---|---|---|
| Si | 1.82 } 2.00 | 1.86 } 2.00 | 1.88 } 2.00 | 1.88 } 2.00 | 1.94 } 2.00 | 1.88 } 2.00 | 1.93 } 2.00 | 1.92 } 2.00 |
| $^{IV}Al$ | .18 } | .14 } | .12 } | .12 } | .06 } | .12 } | .07 } | .08 } |
| $^{VI}Al$ | .03 | .12 | .10 | .14 | .11 | .08 | .03 | .06 |
| Ti | .01 | .01 | .01 | .01 | .02 | .05 | .03 | .03 |
| Cr | .00 | .00 | .00 | .00 | .00 | n.a. | n.a. | .01 |
| Fe | .33 | .38 | .36 | .25 | .32 | .35 | .27 | .33 |
| Mn | .01 | .01 | .01 | .01 | .01 | .01 | .01 | .01 |
| Mg | 1.52 | 1.41 | 1.45 | .89 | .79 | .71 | .84 | .77 |
| Ca | .08 | .08 | .07 | .67 | .68 | .75 | .71 | .74 |
| Na | .01 | .01 | .01 | .00 | .02 | .03 | .02 | .03 |
| | 2.04 | 2.02 | 2.01 | 1.97 | 1.95 | 1.98 | 1.96 | 1.98 |

n.a. = not analyzed

The silicious inclusions also display a disequilibrium relation to the host basalts. Inclusions occur as large fragments of partially resorbed and assimilated silicious "popcorn" granite and fragments of baked sedimentary rocks. Inclusions are particularly common in the Miter and Crescent cinder cones. However, almost every thin section analyzed has evidence of assimilation of at least small amounts of inclusions. The rims of the inclusions commonly display corroded and resorbed glassy rims. The inclusions are evidence that assimilation of material may be an important process in the development of the chemical variation of the Ice Springs basalts.

## STATISTICS

The general chemical affinity of the Ice Springs basalts is tholeiitic. The basalts contain abundant normative plagioclase, hypersthene, and diopside with normative olivine ranging from 2-5% in the Crescent samples to 3-9% in the Terrace samples (Table 7). In order to establish the extent of the chemical variation within the Ice Springs basalts, several statistical tests were performed to evaluate the inter- and intra-eruption variations. These tests included calculations of means, standard deviations, tests of significance (t and F), and correlation coefficients. The data were analyzed at two levels of grouping. First, the samples were classified as belonging to one of the major eruptive units - Crescent, Miter, Pocket, or Terrace. A second classification was developed to subdivide the major groups into subgroups. Based on elevations along the sample traverse, the samples from the Crescent and Terrace cinder cones were divided into early and late eruptive phases. The elevation cutoff points were defined on the basis of major changes in Ti, Fe, and Rb concentration. For the Miter and Pocket cinder cones, no easily determined cutoff points could be located and both of these groups were treated as single units. The lava flows associated with each cinder cone were also classified as subgroups. All in all, 4 major groups and 10 subgroups were considered in the statistical analyses. The basic chemical data and the group classifications are listed in Appendix 1.

Table 7a. Averages and standard deviations of Ice Springs basalts whole rock chemistry.

CRESCENT DATA

| wt% | All Crescent (N=30) | | All Flows (N=6) | | Cinder Early (N=12) | | Cinder Late (N=17) | |
|---|---|---|---|---|---|---|---|---|
| | mean | std.dev. | mean | std.dev. | mean | std.dev. | mean | std.dev. |
| $SiO_2$ | 51.73 | .92 | 51.25 | 1.23 | 52.17 | .70 | 51.20 | .72 |
| $TiO_2$ | 1.63 | .11 | 1.59 | .13 | 1.57 | .04 | 1.76 | .03 |
| $Al_2O_3$ | 15.50 | .38 | 15.42 | .25 | 15.56 | .43 | 15.43 | .27 |
| $Fe_2O_3$ | 1.21 | .07 | 1.17 | .08 | 1.17 | .02 | 1.28 | .02 |
| FeO | 8.34 | .40 | 8.25 | .37 | 8.06 | .16 | 8.81 | .11 |
| MnO | .17 | .01 | .18 | .00 | .17 | .01 | .18 | .01 |
| MgO | 7.35 | .33 | 7.46 | .39 | 7.35 | .26 | 7.27 | .34 |
| CaO | 8.76 | .24 | 8.67 | .40 | 8.70 | .16 | 8.91 | .15 |
| $Na_2O$ | 2.87 | .32 | 2.78 | .35 | 2.85 | .34 | 2.97 | .22 |
| $K_2O$ | 1.38 | .11 | 1.39 | .11 | 1.46 | .03 | 1.26 | .06 |
| $P_2O_5$ | .49 | .04 | .46 | .05 | .47 | .01 | .53 | .02 |
| Loss | .30 | .26 | .42 | .83 | .35 | .20 | .33 | .31 |
| Total | 99.73 | | 99.04 | | 99.88 | | 99.93 | |
| Nb* | 21 | 1.9 | 21 | .9 | 21 | 2.0 | 20 | 1.6 |
| Zr* | 162 | 7.9 | 153 | 5.8 | 163 | 3.6 | 165 | 9.1 |
| Y* | 29 | 1.9 | 28 | 1.3 | 28 | 1.5 | 30 | 1.4 |
| Sr* | 345 | 11.0 | 348 | 9.0 | 338 | 5.6 | 353 | 10.6 |
| Rb* | 28 | 4.6 | 28 | 4.3 | 32 | 2.1 | 23 | 2.3 |
| Th* | 5 | 4.0 | 6 | 2.6 | 6 | 4.0 | 2 | 2.3 |
| Ni* | 136 | 10 | 126 | | 147 | 1.4 | 131 | 2.8 |
| Cr* | 254 | 18 | 230 | | 272 | 2.1 | 249 | 3.5 |

*parts per million

Table 7a. Averages and standard deviations of Ice Springs basalts whole rock chemistry (continued).

MITER DATA

| wt% | All Miter | | All Cinder | | All Flows | | All Pocket (N=9) | |
|---|---|---|---|---|---|---|---|---|
| | mean | std.dev. | mean | std.dev. | mean | std.dev. | mean | std.dev. |
| $SiO_2$ | 50.5 | 1.21 | 50.53 | 1.18 | 49.83 | 1.80 | 51.17 | .83 |
| $TiO_2$ | 1.86 | .18 | 1.88 | .15 | 1.79 | .23 | 1.96 | .03 |
| $Al_2O_3$ | 15.4 | .35 | 15.36 | .44 | 15.26 | .44 | 15.32 | .23 |
| $Fe_2O_3$ | 1.28 | .08 | 1.28 | .06 | 1.25 | .10 | 1.33 | .03 |
| FeO | 9.20 | .57 | 9.21 | .45 | 8.93 | .71 | 9.44 | .06 |
| MnO | .18 | .01 | .18 | .01 | .18 | .01 | .19 | .01 |
| MgO | 7.28 | .42 | 7.21 | .37 | 7.55 | .64 | 7.21 | .36 |
| CaO | 8.88 | .26 | 8.87 | .31 | 9.36 | 1.08 | 8.66 | .14 |
| $Na_2O$ | 2.88 | .33 | 2.91 | .33 | 2.65 | .20 | 2.95 | .22 |
| $K_2O$ | 1.20 | .15 | 1.18 | .14 | 1.27 | .18 | 1.28 | .05 |
| $P_2O_5$ | .55 | .07 | .56 | .06 | .51 | .08 | .56 | .02 |
| Loss | .48 | .50 | .91 | 1.01 | .78 | 1.21 | .17 | .17 |
| Total | 99.69 | | 100.08 | | 99.36 | | 100.24 | |
| Nb* | 21 | 2.3 | 20 | 1.8 | 23 | 1.9 | 20 | 1.8 |
| Zr* | 161 | 7.0 | 163 | 5.8 | 156 | 5.4 | 170 | 6.4 |
| Y* | 29 | 1.7 | 29 | 1.8 | 30 | .8 | 30 | .7 |
| Sr* | 363 | 12.1 | 363 | 11.7 | 362 | 10.7 | 362 | 6.1 |
| Rb* | 23 | 4.2 | 22 | 3.3 | 25 | 5.1 | 23 | 1.0 |
| Th* | 7 | 3.1 | 6 | 3.1 | 8 | 1.9 | 6 | 1.2 |
| Ni* | 127 | | 112 | | 142 | | 124 | |
| Cr* | 221 | | 194 | | 247 | | 199 | |

*parts per million

Table 7a. Average and standard deviations of Ice Springs basalts whole rock chemistry (continued).

| | POCKET DATA | | | | TERRACE DATA | | | |
|---|---|---|---|---|---|---|---|---|
| | All Cinder Pocket (N=7) | | All Flows Pocket (N=2) | | All Terrace (N=24) | | All Flows (N=4) | |
| wt% | mean | std.dev. | mean | std.dev. | mean | st.dev. | mean | st.dev. |
| $SiO_2$ | 51.53 | .31 | 49.93 | .64 | 49.88 | 1.10 | 49.67 | .85 |
| $TiO_2$ | 1.97 | .03 | 1.95 | .03 | 1.88 | .10 | 1.90 | .04 |
| $Al_2O_3$ | 15.29 | .22 | 15.44 | .18 | 15.28 | .35 | 15.66 | .26 |
| $Fe_2O_3$ | 1.34 | .03 | 1.32 | .01 | 1.32 | .06 | 1.37 | .01 |
| FeO | 9.45 | .06 | 9.45 | .04 | 9.10 | .34 | 9.39 | .10 |
| MnO | .18 | .00 | .19 | .00 | .18 | .02 | .17 | .03 |
| MgO | 7.04 | .09 | 7.83 | .08 | 7.36 | .54 | 8.15 | .61 |
| CaO | 8.64 | .13 | 8.75 | .04 | 9.06 | .35 | 8.95 | .13 |
| $Na_2O$ | 3.00 | .20 | 2.76 | .01 | 2.77 | .28 | 2.76 | .19 |
| $K_2O$ | 1.28 | .06 | 1.26 | .01 | 1.14 | .15 | 1.13 | .12 |
| $P_2O_5$ | .57 | .01 | 0.54 | 0.01 | .55 | .04 | .54 | .02 |
| Loss | .13 | .16 | .32 | .02 | .61 | .46 | .03 | .05 |
| Total | 100.42 | | 99.74 | | 99.13 | | 99.89 | |
| Nb* | 20 | 1.8 | 21 | .00 | 20 | 1.7 | 20 | 2.3 |
| Zr* | 172 | 4.6 | 161 | .50 | 151 | 13 | 150 | 11.3 |
| Y* | 30 | .7 | 30 | .00 | 30 | 1.8 | 30 | 1.5 |
| Sr* | 362 | 6.5 | 363 | .5 | 369 | 13.5 | 371 | 8.3 |
| Rb* | 23 | 1.0 | 23 | 1.0 | 22 | 3.3 | 20 | 1.5 |
| Th* | 5 | 1.2 | 6 | .5 | 5 | 2.4 | 3 | 1.5 |
| Ni* | 128 | | 121 | | 116 | | 125 | |
| Cr* | 196 | | 203 | | 205 | | 220 | |

*parts per million

Table 7a. Average and standard deviations of Ice Springs basalts whole rock chemistry (continued).

| | TERRACE | | | |
|---|---|---|---|---|
| | Cinder Early (N=10) | | Cinder Late (N=10) | |
| wt% | mean | st.dev. | mean | st.dev. |
| $SiO_2$ | 49.21 | .91 | 50.11 | .61 |
| $TiO_2$ | 1.86 | .05 | 1.92 | .03 |
| $Al_2O_3$ | 15.30 | .32 | 15.07 | .22 |
| $Fe_2O_3$ | 1.32 | .03 | 1.32 | .02 |
| FeO | 9.06 | .20 | 9.07 | .12 |
| MnO | .19 | .01 | .19 | .01 |
| MgO | 7.54 | .15 | 6.94 | .25 |
| CaO | 9.28 | .38 | 8.96 | .25 |
| $Na_2O$ | 2.85 | .25 | 2.68 | .32 |
| $K_2O$ | 1.02 | .05 | 1.21 | .08 |
| $P_2O_5$ | .53 | .01 | .59 | .01 |
| Loss | 1.0 | .45 | .70 | .29 |
| Total | 99.16 | | 100.04 | |
| Nb* | 20 | 1.4 | 20 | 1.2 |
| Zr* | 139 | 2.9 | 162 | 8.4 |
| Y* | 29 | 1.2 | 31 | 1.6 |
| Sr* | 377 | 23 | 369 | 8.4 |
| Rb* | 21 | 2.8 | 23 | 1.4 |
| Th* | 4 | 2.3 | 5 | 1.9 |
| Ni* | | | 108 | |
| Cr* | | | 190 | |

*parts per million

Table 7b. Average normative values (wt%) of Ice Springs basalts whole rock chemistry.

| | All Crescent | All Flows Crescent | Early Crescent | Late Crescent | All Miter | All Flows Miter | All Cinder Miter |
|---|---|---|---|---|---|---|---|
| OR | 8.15 | 8.21 | 8.63 | 7.45 | 7.09 | 7.50 | 6.97 |
| PL | 49.62 | 49.02 | 49.47 | 50.18 | 49.92 | 48.42 | 49.99 |
| (AB) | 24.28 | 23.52 | 24.12 | 25.13 | 24.37 | 22.42 | 24.62 |
| (AN) | 25.34 | 25.49 | 25.35 | 25.05 | 25.55 | 25.99 | 25.37 |
| DI | 12.18 | 11.84 | 12.01 | 12.83 | 12.21 | 13.98 | 12.27 |
| (WO) | 6.23 | 6.06 | 6.15 | 6.55 | 6.23 | 7.14 | 6.25 |
| (EN) | 3.60 | 3.52 | 3.59 | 3.71 | 3.47 | 4.07 | 3.48 |
| (FS) | 2.35 | 2.25 | 2.27 | 2.57 | 2.51 | 2.76 | 2.53 |
| HY | 21.32 | 21.29 | 22.71 | 18.23 | 18.12 | 15.73 | 18.29 |
| (EN) | 12.90 | 12.98 | 13.92 | 10.77 | 10.52 | 9.38 | 10.58 |
| (FS) | 8.42 | 8.31 | 8.79 | 7.46 | 7.60 | 6.36 | 7.71 |
| OL | 2.17 | 2.48 | .94 | 4.49 | 5.21 | 6.55 | 4.92 |
| (FO) | 1.26 | 1.45 | .55 | 2.55 | 2.90 | 3.75 | 2.73 |
| (FA) | .91 | 1.03 | .39 | 1.94 | 2.31 | 2.80 | 2.19 |
| Mt | 1.75 | 1.70 | 1.7 | 1.86 | 1.86 | 1.81 | 1.86 |
| IL | 3.10 | 3.02 | 2.98 | 3.34 | 3.53 | 3.40 | 3.57 |
| AP | 1.16 | 1.09 | 1.11 | 1.26 | 1.30 | 1.21 | 1.33 |
| rest | .30 | .42 | .35 | .33 | .48 | .78 | .91 |
| Total | 99.45 | 99.06 | 99.90 | 99.96 | 99.72 | 99.39 | 100.11 |

Table 7b. Average normative values (wt%) of Ice Springs basalts whole rock chemistry (continued).

| | All Pocket | All Cinder Pocket | All Flows Pocket | All Terrace | All Flows Terrace | Early Terrace | Late Terrace |
|---|---|---|---|---|---|---|---|
| OR | 7.56 | 7.56 | 7.45 | 6.74 | 6.68 | 6.03 | 7.15 |
| PL | 49.74 | 49.86 | 49.37 | 49.33 | 50.36 | 50.06 | 48.19 |
| (AB) | 24.96 | 25.38 | 23.35 | 23.44 | 23.35 | 24.12 | 22.68 |
| (AN) | 24.78 | 24.47 | 26.02 | 25.89 | 27.00 | 25.94 | 25.52 |
| DI | 11.90 | 12.02 | 11.33 | 12.64 | 11.32 | 13.59 | 12.35 |
| (WO) | 6.06 | 6.12 | 5.79 | 6.46 | 5.79 | 6.94 | 6.30 |
| (EN) | 3.35 | 3.35 | 3.28 | 3.64 | 3.34 | 3.95 | 3.49 |
| (FS) | 2.49 | 2.55 | 2.26 | 2.55 | 2.19 | 2.70 | 2.57 |
| HY | 19.67 | 20.77 | 16.42 | 17.79 | 14.88 | 13.29 | 21.97 |
| (EN) | 11.28 | 11.80 | 9.74 | 10.46 | 8.99 | 7.90 | 12.64 |
| (FS) | 8.39 | 8.97 | 6.69 | 7.33 | 5.89 | 5.39 | 9.32 |
| OL | 4.24 | 3.06 | 7.98 | 5.26 | 9.61 | 8.51 | 1.47 |
| (FO) | 2.33 | 1.67 | 4.54 | 2.97 | 5.58 | 4.86 | .81 |
| (FA) | 1.91 | 1.40 | 3.44 | 2.29 | 4.03 | 3.66 | .66 |
| Mt | 1.93 | 1.94 | 1.91 | 1.91 | 1.99 | 1.91 | 1.91 |
| IL | 3.72 | 3.74 | 3.70 | 3.57 | 3.61 | 3.53 | 3.65 |
| AP | 1.33 | 1.35 | 1.28 | 1.30 | 1.28 | 1.26 | 1.40 |
| rest | .17 | .13 | .32 | .61 | .03 | 1.0 | .70 |
| Total | 100.27 | 100.45 | 99.77 | 99.16 | 99.75 | 99.19 | 98.79 |

Preliminary statistical analysis involved informal screening of the data to remove outliers. The criteria for an outlier was a loss content greater than 2% and/or an analytical total exceeding 103% (ISB 4, 7, 55, 43, 40). Removal of the high loss samples is justified because the high loss values indicate sample contamination, post eruption oxidation, or bad analytical technique. Calculated univariant statistical values of means and standard deviations for the 4 major data groups and the 10 subgroups are given in Table 7. These results indicate that in terms of mean values, the chemical compositions of the various groups of Ice Springs basalts appear significantly different. Three techniques proved useful in quantitatively testing the significance of differences between the group means. First, t-tests were calculated to test the equality of means. Second, F-tests (ANOVA) were calculated to test the inequality of means. And lastly, graphical analysis of data histograms and correlations were plotted to display the data distributions between groups. More elaborate multivariant statistical techniques were attempted, but the basic assumptions necessary for the valid use of the multivariant analyses appeared violated. In particular, the variance-covariance matrices of the data distributions were seen to be variable in size and therefore, comparison of multiple variances of different magnitudes is improper (Davis, 1974).

Comparison of Means

The t-test used is a valid technique to compare group means for groups having separate variances (Brownlee, 1965). The calculation

techniques and results of the test for Fe, Ti, Rb, and Sr are shown in the t-value matrix as Table 8. Similar results were obtained for Si, K, P, and Zr. The elements labeled have significantly different mean values at the calculated degrees of freedom and at the 95% confidence interval. These results clearly show that all possible groupings of Crescent material are significantly different from the other eruptive groups. Also, the development of intra-eruption variations are significantly developed primarily for the Crescent and Terrace subgroups.

To support the conclusions of the t-tests, a one-way analysis of variance was performed for the two data groupings. The hypothesis being tested is that at least one mean value of the groups in the analysis is different. The calculation techniques and results of the tests are listed in Table 9. These results confirm the t-tests and indicate that at least one group of Ice Springs eruptive phases is significantly different with regards to Si, Ti, Mn, Fe, K, P, Zr, Sr, and Rb.

Graphical presentation of the data distributions in frequency histograms clearly supports the conclusions of the t and F tests. When taken as a whole, the entire Ice Springs data distribution appears normally shaped with regards to Si, Al, Mg, Mn, Na, Ca, Y, and Nb as shown by $SiO_2$ and MgO in Figure 4. However, the distribution shapes for Ti, Fe, K, P, Rb, and Sr approach a bimodal distribution as shown by $TiO_2$ and FeO in Figure 5. The distribution of Rb, Sr, Fe, and Ti between the early and late Crescent as well as between the Crescent and other eruptive units also show a clear bimodal distribution. This

Table 8a. "t-value" matrix for major eruptive groups for Ti, Fe, Rb, and Sr at the 95% confidence level, where:

$$\text{"t"} = (X_1 - X_2)/\left(\frac{\sigma_1^2}{n_1} + \frac{\sigma_2^2}{n_2}\right)^{1/2} \quad ; \quad \text{D.F.} = \left[\frac{C^2}{n_1 - 1} + \frac{(1-C)^2}{n_2 - 1}\right]^{-1} \quad ;$$

and

$$C = \frac{\text{var}(X_1)}{\text{var}(X_1 + X_2)} = \frac{\sigma_1/n_1}{\sigma_{1/n_1}^2 + \sigma_{2/n_2}^2}$$

$\overline{X}_i$ = mean; $\sigma_i$ = std. dev.; and $n_i$ = number in group.

Significantly different values labeled (95% level)

| | CRESCENT | MITER | POCKET | TERRACE |
|---|---|---|---|---|
| MITER | Ti Fe<br>Rb Sr | | | |
| POCKET | Ti Fe<br>Rb Sr | | | |
| TERRACE | Ti Fe<br>Rb Sr | | Ti Fe | |

Table 8b. "t-value" matrix for all eruptive subgroups with significantly different values labeled (95% confidence level.

| | Early Crescent | | Late Crescent | | Early Terrace | | Late Terrace | | Miter Cinder | | Pocket Cinder | | Crescent Lavas | | Terrace Laves | | Miter Lavas | Pocket Lavas |
|---|---|---|---|---|---|---|---|---|---|---|---|---|---|---|---|---|---|---|
| Late Crescent | Ti Rb | Fe Sr | | | | | | | | | | | | | | | | |
| Early Terrace | Ti Rb | Fe Sr | Ti Rb | Fe Sr | | | | | | | | | | | | | | |
| Late Terrace | Ti Rb | Fe Sr | Ti | Fe Sr | Ti | | | | | | | | | | | | | |
| Miter Cinder | Ti Rb | Fe Sr | Ti | Fe Sr | | | | | | | | | | | | | | |
| Pocket Cinder | Ti Rb | Fe Sr | Ti | Fe Sr | Ti Rb | Fe Sr | Ti | Fe Sr | Ti | Fe | | | | | | | | |
| Crescent Lavas | | Sr | Ti Rb | Fe | Ti Rb | Fe Sr | Ti Rb | Fe Sr | Ti Rb | Fe Sr | Ti Rb | Fe Sr | | | | | | |
| Terrace Lavas | Ti Rb | Fe Sr | Rb | Fe Sr | | Fe | Rb | Fe | | | Ti Rb | | Ti Rb | Fe Sr | | | | |
| Miter Lavas | Rb | Fe Sr | | | | | | | | | | | | Fe | | | | |
| Pocket Lavas | Ti Rb | Fe Sr | Ti | Fe Sr | Ti | Fe | | Fe Sr | | | | | Ti Rb | Fe Sr | | | | |

Table 9. F-values for ANOVA Analysis

| | For 10 Subgroups | For 4 Main Groups |
|---|---|---|
| | F | F |
| $SiO_2$ | 7.65 * | 8.58 * |
| $TiO_2$ | 16.86 * | 32.29 * |
| $Al_2O_3$ | 2.41 | 1.11 |
| FeO | 17.03 * | 29.10 * |
| MnO | 5.20 * | 6.43 * |
| MgO | 4.22 * | 0.24 |
| CaO | 2.55 | 4.79 * |
| $Na_2O$ | 2.11 | 1.50 |
| $K_2O$ | 15.55 * | 19.20 * |
| $P_2O_5$ | 11.10 * | 12.20 * |
| Nb | 1.96 | 1.50 |
| Zr | 15.10 * | 14.21 * |
| Y | 4.45 * | 2.19 |
| Sr | 8.93 * | 13.55 * |
| Rb | 11.86 * | 14.38 * |
| | D.F.=9&76 | D.F.=3&86 |
| | Significance levels | Significance levels |
| | F > 2.00 for 95% | F > 2.75 for 95% |
| | 2.70 for 99% | 4.22 for 99% |

* Significant difference between at least one mean at the 99% significance level.

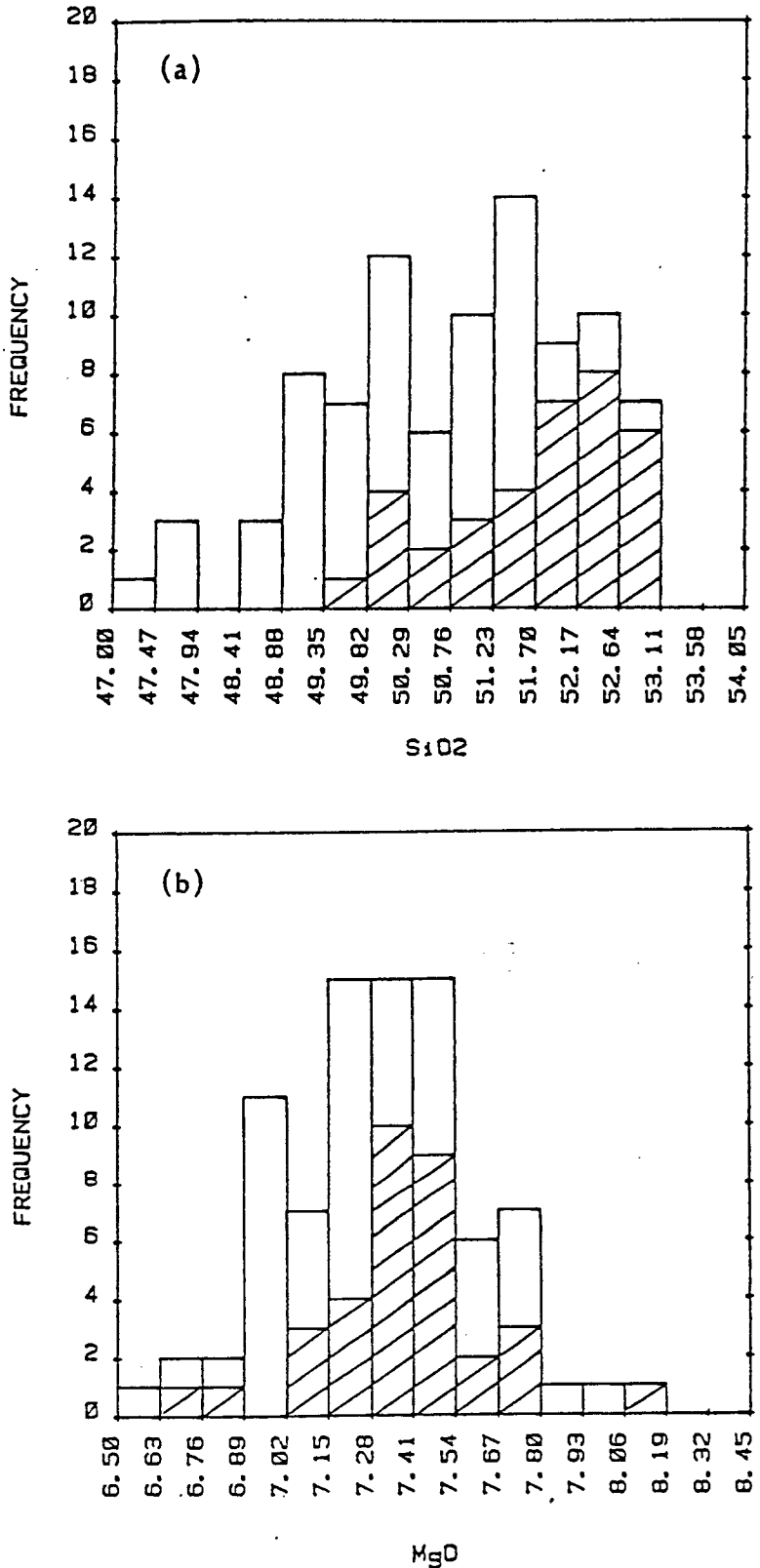


Figure 4. a) Frequency histogram of $SiO_2$ distribution for all Ice Springs data. Shaded area is distribution for Crescent data only. b) Frequency histogram of MgO distribution for all Ice Springs data. Shaded area is distribution for Crescent data only.

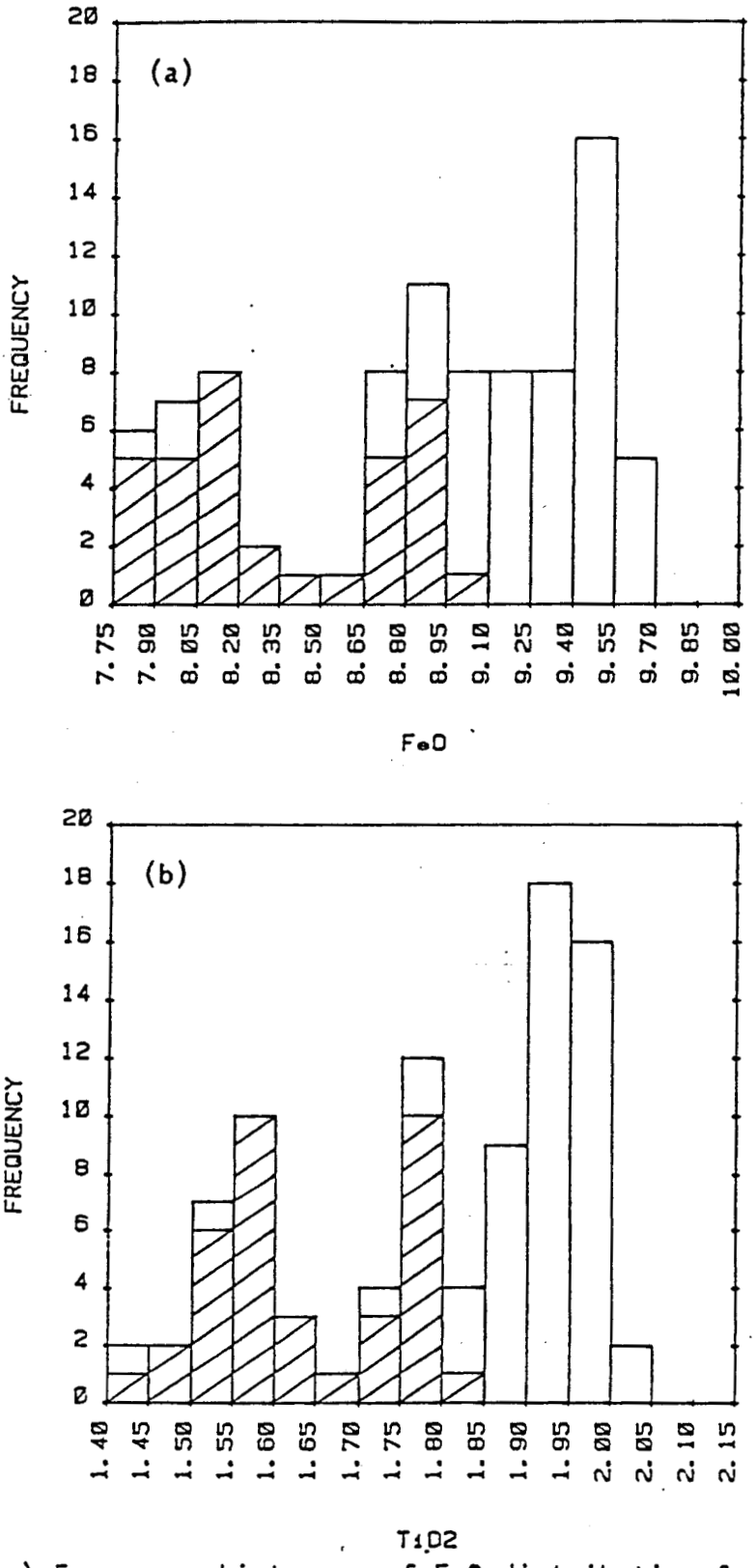


Figure 5. a) Frequency histogram of FeO distribution for all Ice. Springs data. Shaded area is distribution for Crescent data only. b) Frequency histogram of $TiO_2$ distribution for all Ice Springs data. Shaded area is distribution for Crescent data only.

bimodal distribution of the data between the Crescent and the other groups and within the Crescent graphically supports the t-test and F-test analysis that significant chemical variation exists in the Ice Springs volcanic field.

Correlations

To assess the direction and magnitude of the chemical variations, correlation coefficients were calculated for the Ice Springs data. The statistically significant coefficients at the 95% and 99% confidence intervals for all Ice Springs data and for all eruptive subgroups are presented in Table 10. These results identify several correlations of petrological importance. Trends of significant negative correlations exist between the combined elements Ti, Fe, Ca, P, and Sr versus K, Zr, and Rb. Similar negative correlations are developed between Si, Al, and Na versus Mg, Mn, and Y. However, the statistically low confidence of these coefficients and the large analytical error associated with the analysis for these elements limits the importance of the later correlations. The coherence of the groups of elements indicates that an important process or combination of processes must be acting on the Ice Springs magma system. Similarly, the appearance of these same significant trends during intra-eruptions as within the Crescent or Terrace subgroups indicates the consistency of the differentiation processes. The lack of significant correlations in the Miter with regards to Sr and Ca while still displaying significant coefficients with Rb, Fe, Ti, and Mg indicate minor perturbations in the processes. The lack of significant correlations in the Pocket data indicates

Table 10a. Correlation matrix for all Ice Springs data (D.F.=83). For 95% significance level r>.217; for 99% significance level r>.283. Lower left half of diagram is significant at 99% significance level and other values not presented.

| | $SiO_2$ | $TiO_2$ | $Al_2O_3$ | FeO | MnO | MgO | CaO | $Na_2O$ | $K_2O$ | $P_2O_5$ | Nb | Zr | Y | Sr | Rb |
|---|---|---|---|---|---|---|---|---|---|---|---|---|---|---|---|
| $SiO_2$ | | | | | | | | | | | | | | | |
| $TiO_2$ | -.53 | | | | | | | | | | | | | | |
| $Al_2O_3$ | .46 | | | | | | | | | | | | | | |
| FeO | -.52 | .97 | | | | | | | | | | | | | |
| MnO | -.40 | .62 | -.29 | .62 | | | | | | | | | | | |
| MgO | | | .49 | | | | | | | | | | | | |
| CaO | -.31 | .30 | | .37 | | | | | | | | | | | |
| $Na_2O$ | | | | | | | | | | | | | | | |
| $K_2O$ | .75 | -.75 | | -.77 | -.56 | | -.53 | | | | | | | | |
| $P_2O_5$ | -.42 | .90 | | .86 | .57 | -.33 | .35 | | -.66 | | | | | | |
| Nb | | | | | | | | | | | | | | | |
| Zr | .40 | | | | | -.40 | -.51 | | .47 | | | | | | |
| Y | | .51 | | .53 | | | | | | .54 | | .32 | | | |
| Sr | -.65 | .66 | -.29 | .63 | .47 | | .58 | | -.75 | .62 | | | .34 | | |
| Rb | .62 | -.84 | | -.85 | -.59 | | -.47 | | .85 | -.74 | | .33 | -.34 | -.68 | |

10b. Correlation matrix for all Crescent data (D.F. = 32). For 95% significance level, r>.349; for 99% confidence level r<.449. Lower left of diagram is significant at 99% level; upper right of diagram is significant at 95%.

| | $SiO_2$ | $TiO_2$ | $Al_2O_3$ | FeO | MnO | MgO | CaO | $Na_2O$ | $K_2O$ | $P_2O_5$ | Nb | Zr | Y | Sr | Rb |
|---|---|---|---|---|---|---|---|---|---|---|---|---|---|---|---|
| $SiO_2$ | | -.42 | .43 | -.44 | -.35 | | | | | | | | | | |
| $TiO_2$ | | | | | | | | | | | | | | | |
| $Al_2O_3$ | | | | | | | | | | | | | | | |
| FeO | | .98 | | | | | | | | | -.39 | | | | |
| MnO | | .78 | | .82 | | | .44 | | | | | | | | |
| MgO | | | | | | | | | | | | | | | |
| CaO | | .54 | | .54 | | | | | | | | | | | |
| $Na_2O$ | | | | | | | | | | .41 | | | | | |
| $K_2O$ | .62 | -.88 | | -.90 | -.77 | | -.49 | | | | | | | | |
| $P_2O_5$ | | .86 | | .83 | .60 | | .61 | | -.72 | | | .36 | | | |
| Nb | | | | | | | | | | | | | | | |
| Zr | | | | | | | | | | | | | .36 | | |
| Y | | .64 | | .63 | .40 | | | | | .64 | | | | .40 | -.40 |
| Sr | | .46 | | .52 | .58 | | .50 | | -.67 | .46 | | | | | |
| Rb | | -.78 | | -.83 | -.72 | | -.57 | | .83 | -.67 | | | | -.57 | |

Table 10c. Correlation matrix for all miter data (D.F. = 15). For 95% significance level, r>.482; for 99% significance level r>.606; significance levels plotted as in 10b.

| | $SiO_2$ | $TiO_2$ | $Al_2O_3$ | FeO | MnO | MgO | CaO | $Na_2O$ | $K_2O$ | $P_2O_5$ | Nb | Zr | Y | Sr | Rb |
|---|---|---|---|---|---|---|---|---|---|---|---|---|---|---|---|
| $SiO_2$ | | | .53 | | | | | | .57 | | | | -.49 | | |
| $TiO_2$ | | | | | | | | | | | | | | | |
| $Al_2O_3$ | | | | | | | | | | | | | | | |
| FeO | | .99 | | | | | | | | | | | | | |
| MnO | | .81 | | .83 | | | | | | | | | | | |
| MgO | | -.62 | .75 | -.64 | -.72 | | | | | -.59 | | | | | .60 |
| CaO | | | | | | | | | | | | | | | |
| $Na_2O$ | | | | | | | | | | | | | | | |
| $K_2O$ | | -.77 | | -.78 | | | | | | | | | | -.49 | |
| $P_2O_5$ | | .95 | | .93 | .77 | | | | | | | | | .58 | |
| Nb | | | | | | | | | | | | | | | |
| Zr | | | | | | | | | | | | | | | |
| Y | | | | | | | | | | | | | | | |
| Sr | | | | | | | | | | | | | | | |
| Rb | | -.90 | | -.91 | -.66 | | | | .87 | -.88 | | | | | |

Table 10d. Correlation matrix for all Pocket data (D.F. = 7). For 95% significance level, r>.666; for 99% significance level, r>.798; significance levels plotted as in 10b.

| | $SiO_2$ | $TiO_2$ | $Al_2O_3$ | FeO | MnO | MgO | CaO | $Na_2O$ | $K_2O$ | $P_2O_5$ | Nb | Zr | Y | Sr | Rb |
|---|---|---|---|---|---|---|---|---|---|---|---|---|---|---|---|
| $SiO_2$ | | .71 | | | | -.78 | | | | .78 | | | | | |
| $TiO_2$ | | | | | | | | | | | | | | | |
| $Al_2O_3$ | | | | | .69 | | | | | | | | | | |
| FeO | | .86 | | | | | | | | | | | | | |
| MnO | | | | | | | | | | | | | | | |
| MgO | | | | | | | | | | | | | | | |
| CaO | | | | | | | | | | | | | | .74 | |
| $Na_2O$ | | | | | | | | | | | | | | | |
| $K_2O$ | | | | | | | | | | | | | | | |
| $P_2O_5$ | | | | | | | | | | | | .73 | | | |
| Nb | | | | | | | | | | | | | | | |
| Zr | | | | | | | | | | | | | | | |
| Y | | | | | | | | | | | | | | -.80 | |
| Sr | | | | | | | | | | | | | | | |
| Rb | | | | | | | | | | | | | | | |

Table 10e. Correlation matrix for all Terrace data (D.F. = 23) for 95% confidence level, r>.396; for 99% confidence level r>.505; significance levels plotted as in 10b.

| | $SiO_2$ | $TiO_2$ | $Al_2O_3$ | FeO | MnO | MgO | CaO | $Na_2O$ | $K_2O$ | $P_2O_5$ | Nb | Zr | Y | Sr | Rb |
|---|---|---|---|---|---|---|---|---|---|---|---|---|---|---|---|
| $SiO_2$ | | | | | | | -.45 | | | | | | | | .45 |
| $TiO_2$ | | | | | | | | | | | | | .44 | | |
| $Al_2O_3$ | | | | | | | | .44 | | | | | | | |
| FeO | | .85 | | | | | | | -.41 | | | | | | |
| MnO | | | | | | | | | | | | | | | |
| MgO | | | .65 | | | | | | | -.42 | | | | | |
| CaO | | | | | | | | | | | | | | | |
| $Na_2O$ | | | | | | | | | | | | -.41 | -.47 | | |
| $K_2O$ | .65 | | | | | -.53 | -.58 | | | | | | | | |
| $P_2O_5$ | | | | .52 | | | | | | | | | .49 | | |
| Nb | | | | | | | | | | | | | | | |
| Zr | | | | | | -.64 | -.63 | | .82 | | | | | | |
| Y | | | | | | | | | | | | .56 | | | |
| Sr | -.61 | | | | | | .57 | | | -.54 | | | | | -.46 |
| Rb | | -.65 | | -.78 | | | -.53 | | | .73 | | .58 | | | |

short-term homogeneity during eruption, and these results are supported by the small standard deviations of the Pocket subgroups.

For the Ice Springs data, several types of variation diagrams display the intra- and inter-eruption trends. Plots with axes of correlated constituents and correlated ratios of constituents, and also plots of significantly correlated constituents versus a relative eruption elevation, all graphically portray the chemical variations of the Ice Springs basalts. An elevation versus constituent diagram displays the generalized trends of chemical variation as a function of eruptive sequence. The four eruptive units -- the Crescent, Miter, Pocket, and Terrace have been assigned relative elevations based on the relative eruptive sequence. This elevation parameter represents the eruptive sequence from the oldest Crescent (highest) to the youngest Terrace (lowest). The cinder material within the individual cones is also plotted with the elevation term being the measured vertical distance along the sample traverse. Samples of flow material are plotted at the base of each eruptive sequence-Crescent flows at 400, Miter flows at 300, Pocket flows at 200, and Terrace flows at 100. The absolute time-space positions of the eruptive events is undefinable. But, this relative elevation-plotting technique enables the graphical presentation of relative chemical variations.

Figure 6a, $SiO_2$ versus elevation, shows the general trend for the Ice Springs field to be one of decreasing $SiO_2$ with decreasing age. As can be seen in the enlarged diagram of the Crescent eruption (Fig. 6b), the trend of declining silica content occurs over the development of a single cinder cone as well as over the entire eruptive sequence. Other

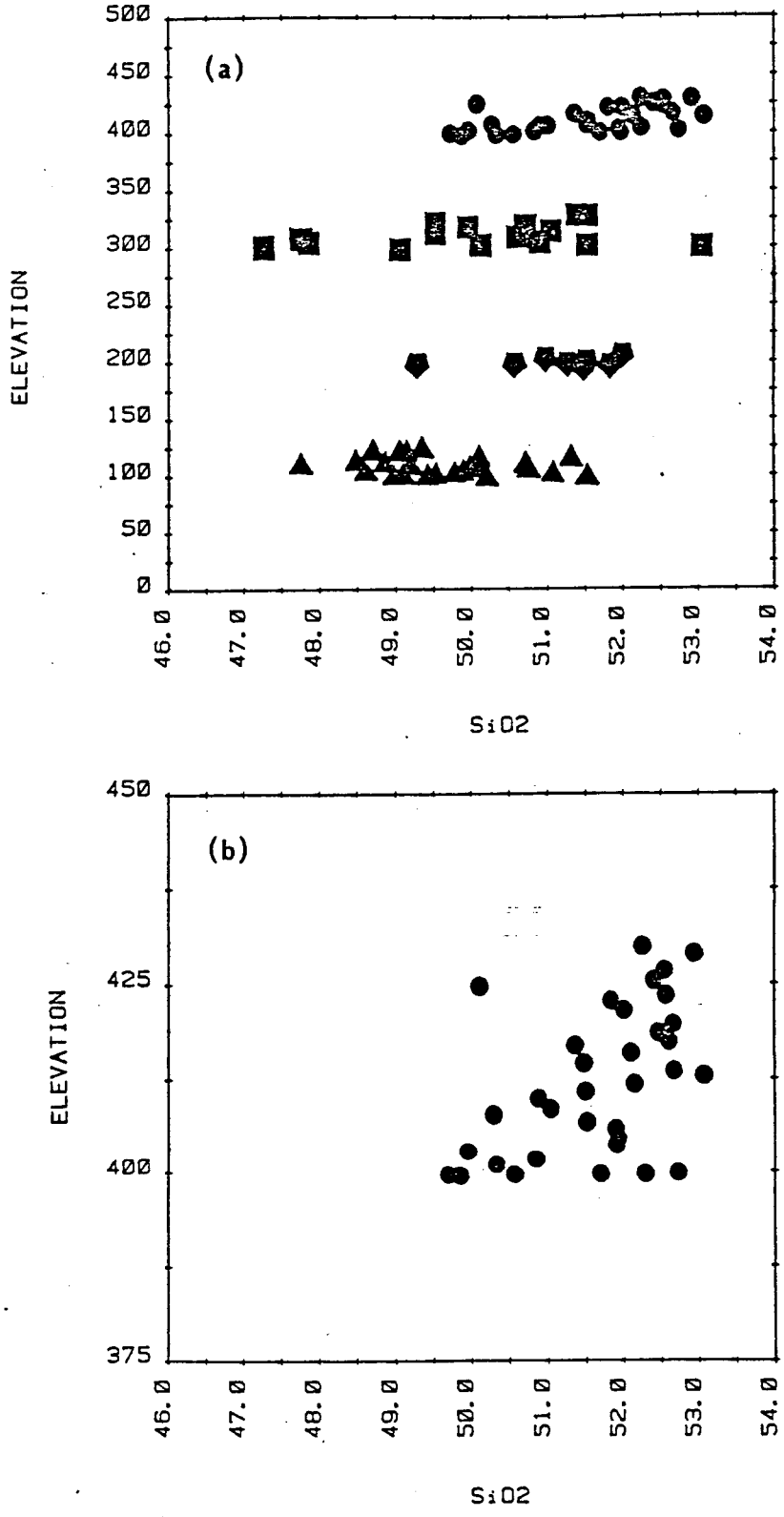


Figure 6. a) Variation diagram of relative elevation versus $SiO_2$ for all data. Solid circles are Crescent data; squares are Miter data; pentagons are Pocket data; and triangles are Terrace data. b) Variation diagram of relative elevation versus $SiO_2$ for Crescent data only.

elements which show trends similar to silica are $K_2O$, Rb, Zr, Ni, Cr, and Rb/Sr. The opposite correlation can be seen with $TiO_2$, FeO, CaO, $P_2O_5$, and Sr. $TiO_2$ versus elevation for all Ice Springs data (Figure 7a) displays rapid $TiO_2$ enrichment overall and also as eruption progresses as in the enlarged Crecent diagram (Figure 7b). Clearly, a process which depletes the late lavas of $SiO_2$, $K_2O$, Rb, Zr, Ni, and Cr while simultaneously enriching them in $TiO_2$, FeO, CaO, $P_2O_5$, and Sr is needed in order to account for the development of the Ice Springs trend.

Other informative correlation diagrams which show the direction and magnitude of chemical variations include: 1) $TiO_2$ and $K_2O$ versus the variation in $SiO_2$ (Figure 8a and 8b), and $K_2O$ and $TiO_2$ versus Rb/Sr (Figure 9a and 9b). In all cases the clustering of the Crescent material at one end of the scale and the Terrace material at the other end is evident. the ordered correlations of these plots indicates that systematic processes are acting on the Ice Springs magma during individual eruptions and over the course of the evolution of the whole volcanic field.

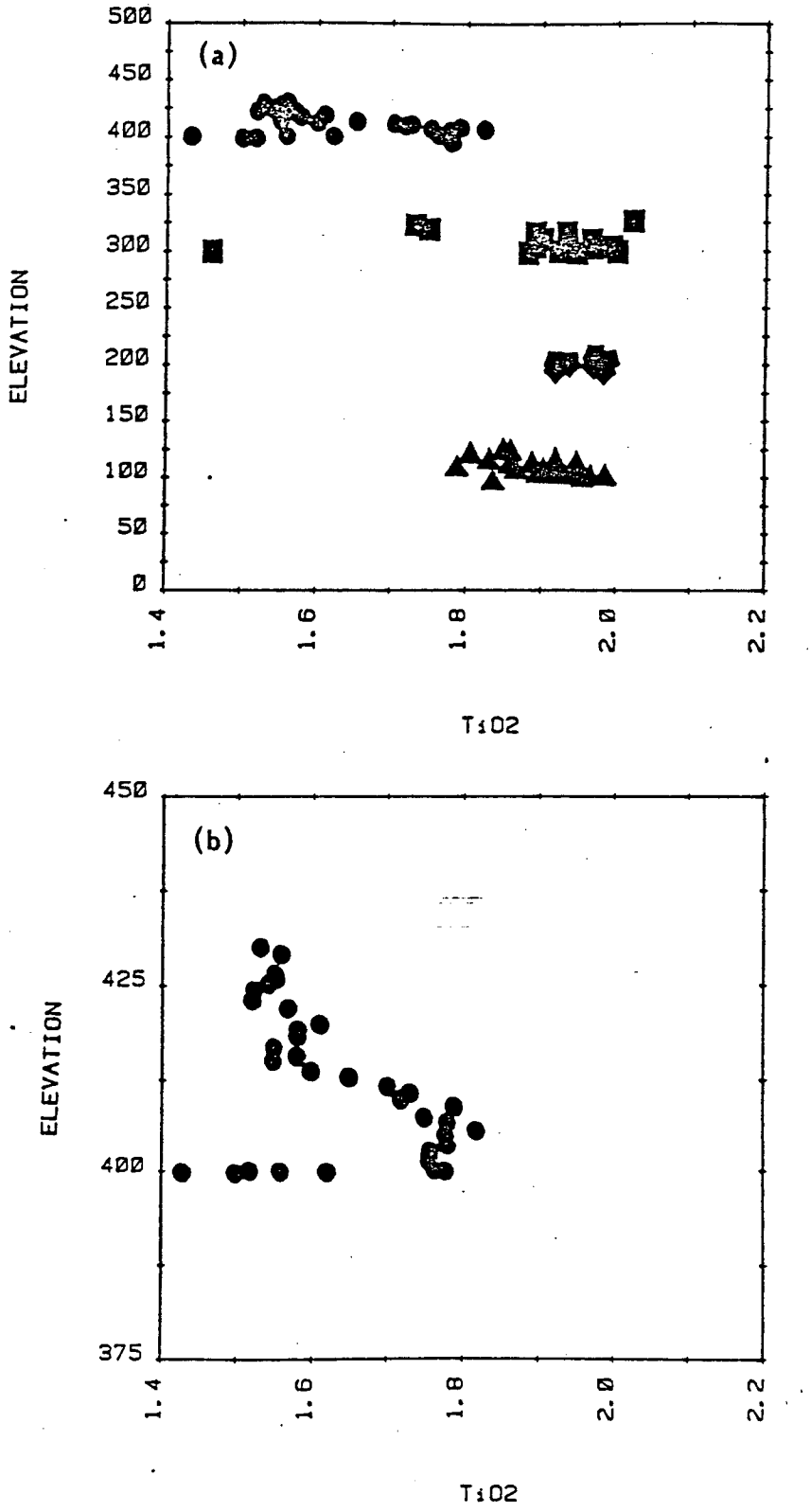


Figure 7. a) Variation diagram of relative elevation versus $TiO_2$ for all data plotted as in Fig. 6. b) Variation diagram of relative elevation versus $TiO_2$ for Crescent data only.

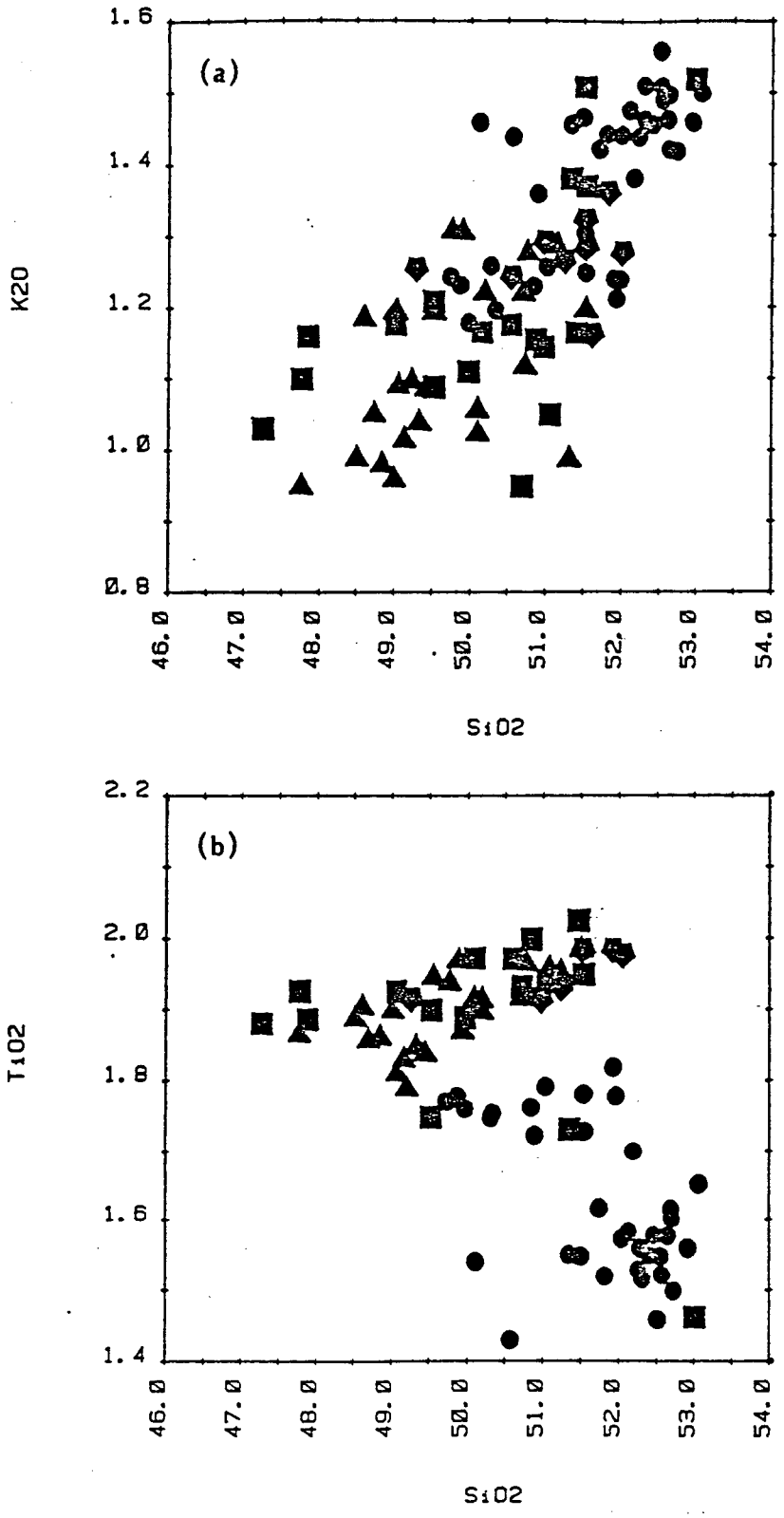


Figure 8. a) Variation diagram of $SiO_2$ versus $K_2O$ for all data with symbols as in Fig. 6. b) Variation diagram of $SiO_2$ versus $TiO_2$ for all data.

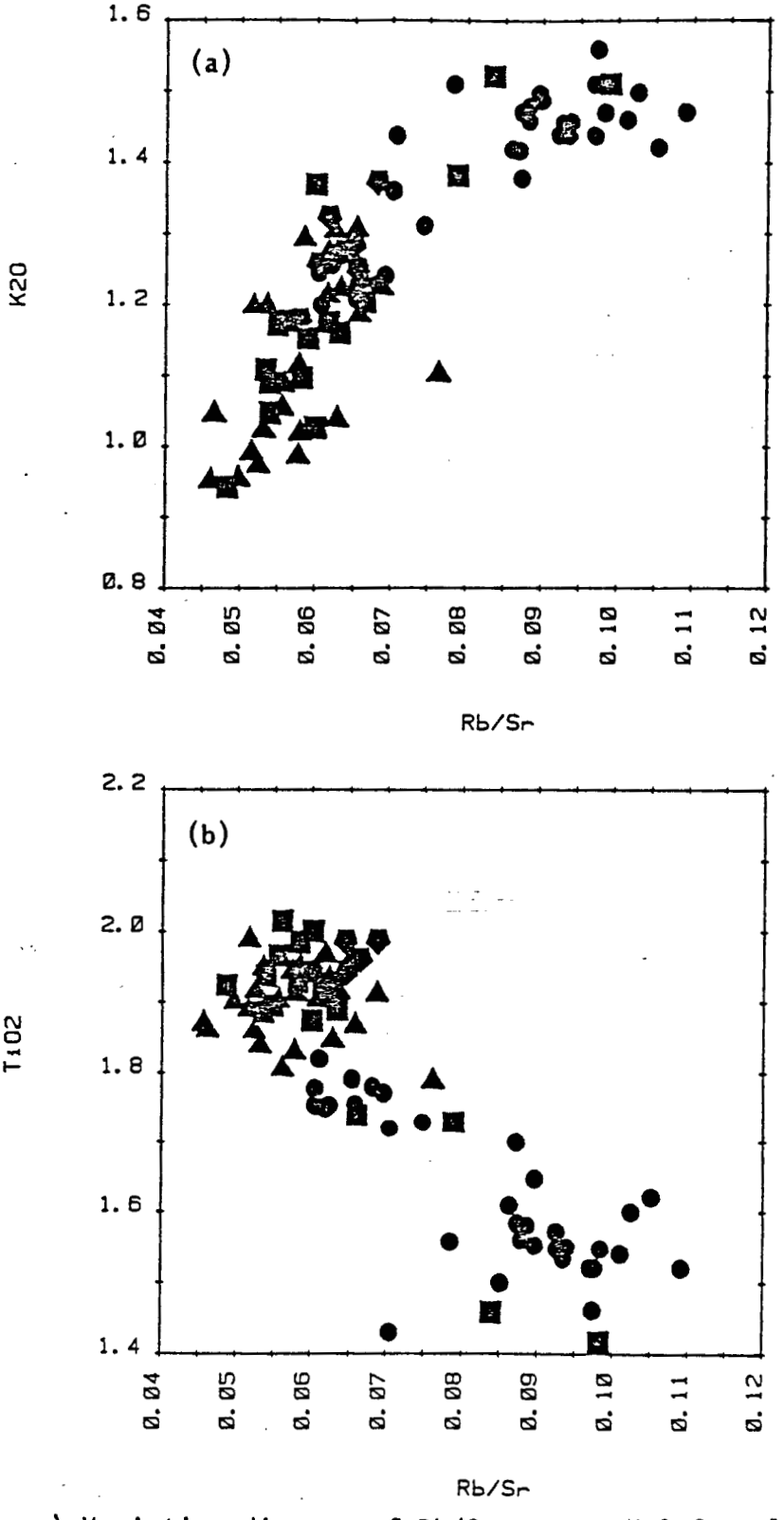


Figure 9. a) Variation diagram of Rb/Sr versus $K_2O$ for all data with symbols as in Fig. 6. b) Variation diagram of Rb/Sr versus $TiO_2$ for all data.

## PHYSICAL PROPERTIES OF THE MAGMA

Because the Ice Springs basalts contain a diverse assemblage of phenocrysts, xenocrysts, xenoliths, and groundmass minerals, a variety of complex fractionation, assimilation, and magma mixing models can be proposed to explain the observed whole rock chemical variations. The physical properties of the Ice Springs magma place constraints on the importance of any proposed processes. To understand the pre-eruptive and eruptive history of the magma, the nature of the structure, heat flow, and crustal configuration of the Black Rock Desert area needs consideration. A variety of recent geophysical and regional tectonic studies have helped place limits on the physical setting of Ice Springs volcanic field (Olson and Smith, 1976; Selk, 1976; Clark, 1974; Carrier, 1979; Serpa, 1980). From these works it can be concluded that the eastern margin of the Great Basin in the Black Rock Desert area is characterized as a region of high heat flow (90 $mW/m^2$), thin crust (25-30 km), extensional tectonics, and high seismic activity. Consideration of these regional properties along with the actual magma properties limits the processes of Ice Springs magmatic differentiation.

### Temperature

Table 11 summarizes the geothermometry data for the Ice Springs basalts. Three potential geothermometers were calculated to estimate groundmass and megacryst equilibrium temperatures. The

Table 11. Summary of calculated geothermometers.

| | Technique | Temperatures °C Crescent | Miter | Pocket | Terrace |
|---|---|---|---|---|---|
| 1. | Olivine-Clinopyroxene (±39°@1bar) | 1006 | 1019 | 1017 | 999 |
| 2. | Fe-Ti Oxides (±30°) | 870 | 955 | --- | 790 |
| | (log $fO_2$) | (-12.8) | (-11.1) | --- | (-15.0) |
| 3. | CPX-OPX (±60°) | 1303 | --- | --- | --- |

1. Powell and Powell (1974)
2. Buddington and Lindsley (1964)
3. Wood and Banno (1973)

olivine-clinopyroxene geothermometer of Powell and Powell (1974) indicates that no significant systematic temperature variation exists within the Ice Springs eruptive sequence. Three pairs of coexisting ilmenites and magnetites were used to calculate temperatures and oxygen fugacities (Buddington and Lindsley, 1964). Only one analysis from the Miter eruption gave a reasonable result and the estimated temperature of 950°C and an oxygen fugacity of $10^{-11.1}$ agrees well with the olivine-clinopyroxene groundmass temperature of 1000°C with oxygen fugacities slightly above the FMQ oxygen buffer. For the megacryst assemblage, the orthopyroxene-clinopyroxene geothermometer of Wood and Banno (1973) was used to calculate an equilbrium temperature between coexisting orthopyroxene megacryst and a clinopyroxene inclusion in megacryst ISB-103. Assuming equilibrium between the pair, a temperature of 1300°C was calculated for the assemblage. This result, along with the chemical and petrologic evidence of disequilibrium with the host basalts suggest a deep source for the megacrysts. Orthopyroxene-olivine phase relations are sensitive to changes in composition, total pressure, and water pressure (Deer et al., 1977). At pressures above 1.3 kbars, fosterite and enstatite form a eutectic relation (Chen and Presnall, 1975). The presence of a homogeneous aluminum rich orthopyroxene in reaction relation to groundmass olivine indicates that the orthopyroxene must have initially formed at pressures exceeding 1.3 kbars. Subsequent movement to lower pressures allowed the development of the olivine reaction rim on the orthopyroxene with the breakdown of the eutectic relations.

Flow Regimens

Knowing that the temperature distribution must have been between 1300°C and 1000°C during the later development of the magma, a variety of temperature and composition dependent properties of the magmas can be calculated. These include density, viscosity, and a variety of additional thermophysical properties listed in Appendix 2. Most of the inter-eruption variations in these properties are insignificant; however, the compositional and temperature effects on density distributions have important implications concerning the physical state of the magma chamber. The petrographic textural analysis suggests that the magma was turbulent during ascent to the surface. However, the compositonal variation within the eruptions has suggested tapping of a zoned magma chamber. A quantitative approach to understanding the magma flow regimen can be calculated using fluid mass transport principles. the technique is to calculate an effective Rayleigh number for the magma system (Turner, 1973). The effective Rayleigh number represents the estimate of balance of buoyant and viscous forces created by thermal and compositional gradients in the magma. The effective Rayleigh number is then the difference between the thermal and compositional (solutal) Rayleigh numbers. The equations and values used in the calculations are shown in Appendix 3. The important variables to consider in these calculations are the thermal and compositional gradients and also the shape of the magma chamber. If the compositional gradient of the chamber is approximated by the density contrast between the early and late erupted material, than the temperature gradients necessary to maintain convection for various

chamber configurations can be calculated. For the Ice Springs system, the density contrast between early and late erupted material is approximately .02 gm/cc. With a short cylindrical magma chamber, a temperature gradient in the vicinity of 200° is needed to maintain convection; However, if the magma chamber elongates, the temperature gradient necessary to maintain convection quickly falls to values approaching 0°. The shape of intrusives moving through the crust at relatively shallow depths or at high magmatic pressures is typically cylindrical or pipe-like (Williams and McBirney, 1979). Also, the above calculations do not consider any horizontal compositional or thermal gradients and these additional gradients would act to enhance convection. Therefore, for the Ice Springs magma system, the flow regiment during its preeruptive history was likely a strongly convecting elongate magma chamber.

## MODELS OF PETROGENESIS

Any model called upon to explain the chemical variation within the Ice Springs basalts must be compatible with the observed physical, chemical, and mineralogical properties of the observed rocks. These properties include: 1) moderate to high temperatures around 1300°C with pressures exceeding 1.3 kbars during the early evolution of the magma body, 2) temperatures approaching 1000°C during crystallizaton at the surface, 3) moderate crystallization rates for microphenocryst phases prior to eruption with increasingly rapid crystallization rates for all phases after eruption, 4) early generation of plagioclase xenocrysts followed by formation of microphenocrysts, 5) possible assimilation of silicious country rock during magma ascent through the crust, 6) systematic chemical variations over the total eruptive sequence and within individual eruptions displayed by decreasing Si, K, Zr, Rb, Ni, and Cr with increasing Ti, Fe, Ca, P, and Sr, and 7) systematic isotopic variations including $^{87}Sr/^{86}Sr$ increases with decreasing age and also variations in the amounts of extraneous argon.

Previous proposed models for the evolution of the Ice Springs volcanic field have included: 1) tapping of a zoned magma chamber with concurrent fractional crystallization of orthopyroxene to explain major element variations (Condie and Barsky, 1972), 2) injection of new batches of mantle derived magma prior to eruption to account for trace element variations (Condie and Barsky, 1972), 3) magma mixing and

assimilation of crustal material to account for the 87Sr/86Sr isotopic data (Puskar and Condie, 1973), and 4) variations in magma generation mechanism including partial melting and/or subequant mixing of residual magmas to explain the major element data (Hoover, 1974).

The Ice Springs basalts do not represent primary melts derived directly from the mantle. The average magnesium numbers (100Mg/Mg+Fe Mole%) for the Ice Springs basalts vary from 61 for the Crescent to 59 for the Miter and Terrace to 58 for the Pocket eruptive units. These values are below the generally acceptable lower limit of 65 for liquids considered to be in equilibrium with mantle olivine (Roeder and Emslie, 1970). The simplest explanation is that olivine has been removed in transit from the source region to the surface. For the Ice Springs basalts, the addition of 17 to 20% olivine is necessary to generate a primitive magma which could be in equilibrium with mantle olivine. These calculations (Irvine, 1979) are summarized in Table 12. A simple addition-subtraction diagram (Bowen, 1928; Wilcox, 1979) was constructed to predict the percent of melting required to generate the primitive magma from a Pyrolite II source material. These calculations suggest that from 19 to 23% partial melting of mantle material with subsequent 17 to 20% olivine fractionation are likely processes responsible for the early development of Ice Springs magmas. Variations in these processes, such as increases in fractionation and partial melting or deep interaction of magma pulses might then be responsible for the development of chemical trends within the Ice Springs eruptions. To support these conclusions, the trace element data needs consideration.

Table 12. Simple model of "primitive" basalts derived by olivine addition to the modified Ice Springs basalts.

| | "Crescent" | | "Terrace" | |
|---|---|---|---|---|
| %olivine added | 17.5 | Removed from mantle | 21 | Removed from mantle |
| % melted | | 19 | | 23 |
| $SiO_2$ | 50.36 | 42.9 | 48.93 | 42.74 |
| $TiO_2$ | 1.39 | .39 | 1.58 | .27 |
| $Al_2O_3$ | 13.25 | 1.75 | 12.85 | 1.23 |
| $Fe_2O_3$ | 1.03 | 0.00 | 1.11 | 0.00 |
| FeO | 8.59 | 7.92 | 9.33 | 7.45 |
| MnO | 0.15 | 0.13 | 0.15 | 0.13 |
| MgO | 13.67 | 45.24 | 14.72 | 46.97 |
| CaO | 7.49 | 1.49 | 7.60 | 1.12 |
| $Na_2O$ | 2.45 | 0.18 | 2.32 | 0.09 |
| $K_2O$ | 1.18 | 0.00 | 0.96 | 0.00 |
| $P_2O_5$ | 0.42 | 0.00 | 0.46 | 0.00 |
| 100Mg/(Mg+Fe) | 74 | | 75 | |

Trace element data for the Ice Springs basalts indicates substantial modification of the magma since its generation in the mantle. Frey et al. (1977) suggest that values for Ni, Co, and Sc as a result of approximately 20% partial melting of the mantle lherzolite should be 670 ppm for Ni, 80 ppm for Co, and 28 ppm for Sc. Modification of these values by the frationation of 17 to 20% olivine as predicted by the magnesium number calculations would result in Ni, Co, and Sc values of 129 to 169, 33 to 38, and 32 to 33 ppm respectively. These Ni and Co values agree well with the Ice Springs values (Condie and Barsky, 1972) of 125 and 36 ppm. However, the Sc value, 60 ppm, is significantly different than the predicted value for simple fractionation of olivine. This unexplained trace element variation in Sc and the additional major element variations in Ti, Fe, and K suggests that other processes besides mantle or deep magmatic processes must be involved in creating the observed Ice Springs trends.

## Shallow Magmatic Processes

Near surface differentiation processes can be tested using major element, trace element, and isotopic data. A variety of major element fractionation paths were tested using the interactive computer program XLFRAC (Stormer and Nicholls, 1978), which tests fractionation paths by calculating linear major element mass balance equations by a least-squares method. The possible paths and phases used in the program are limited by the mineralogy of the parent and derived magmas and by the results of the least-squares calculations. Possible short-term shallow fractionation effects were tested using Terrace

parental material and derived Crescent material and also using parental late erupted Crescent material and derived early erupted Crescent material. If the Ice Springs system represents a single magma chamber or a series of small chambers, then these two fractionation paths will test the feasibility of fractionation during eruption as a mechanism of differentiation. Short-term inter-eruption variations between Terrace and Crescent can be accounted for by several possible fractionation paths including: 1) 2% fractionation of a single magnetite phase, 2) 8% fractionation of olivine (21%), magnetite (24%), and plagioclase (55%), and 3) 6% fractionation of olivine (51%) and plagioclase (49%). Intra-eruption variations such as between late and early Crescent material can be accounted for by similar fraction paths including: 1) 1.5% fractionation of a single magnetite phase, or 2) 4% fractionation of olivine (12%), plagioclase (53%), and magnetite (35%). In terms of major element trends, any of the above processes appear reasonable. Therefore, the additional constraints of the trace element data need consideration.

Using models of trace element behavior developed by Gast (1968) and Shaw (1970) and assuming Rayleigh fractionation, the trace element behavior of the possible fractionation processes can be evaluated. Values of the distribution coefficients were taken from the literature for Rb, Sr, K, Sc, Co, Ni, Cr, and P (Leeman, 1976; Irving, 1978; Frey, 1979). These elements were chosen because of the accuracy of the determination of their distribution coefficients and because these elements show important chemical trends in the Ice Springs basalts (Fig. 10). Calculations of elemental distributions during

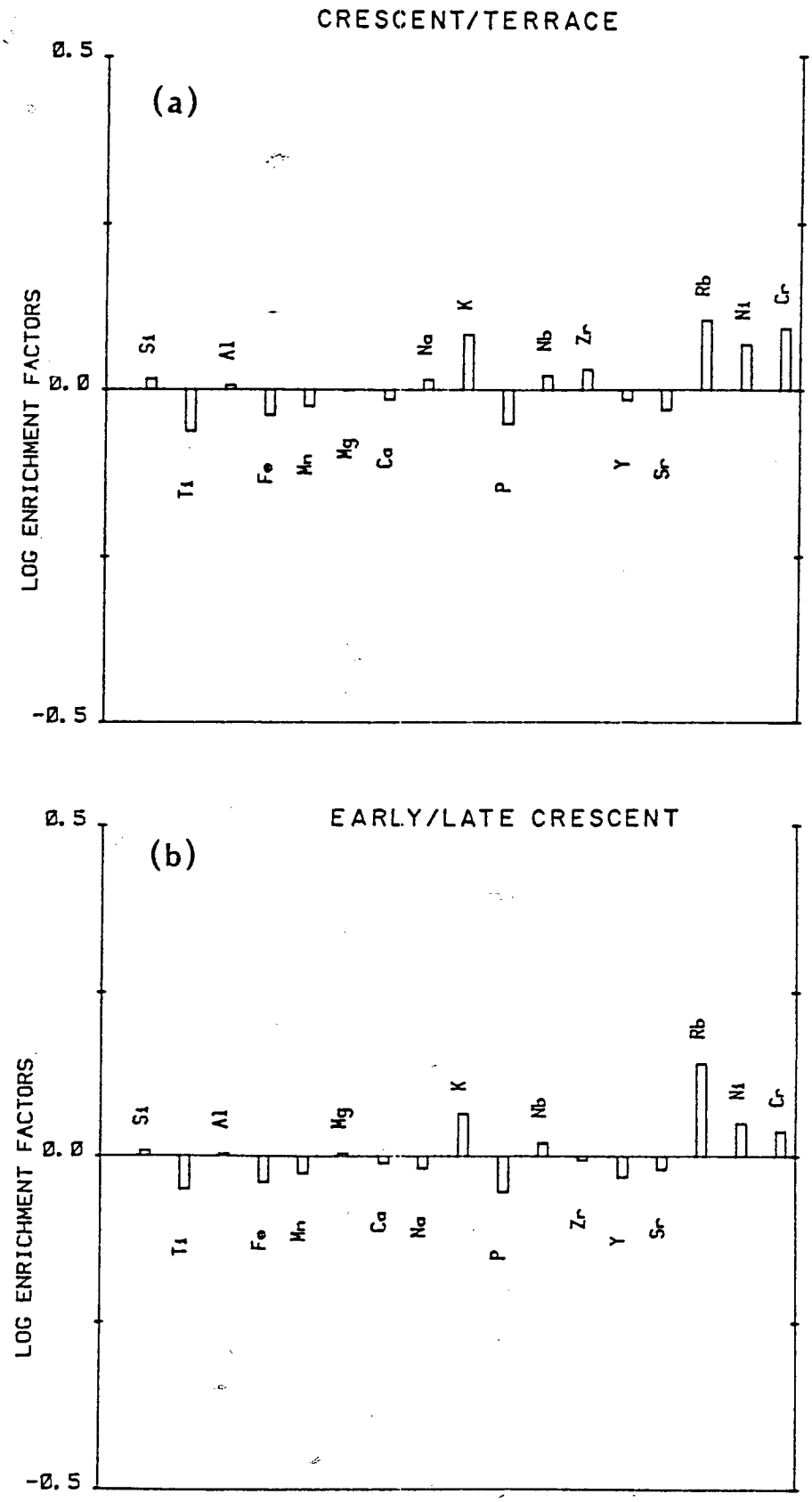


Figure 10a. Log enrichment diagram model for all Ice Springs data calculated as log (concentration Crescent/concentration Terrace). 10b. Log enriched diagram mode for Crescent data only calculated as above.

fractionation of the proposed mineral assemblages are illustrated in Figure 11. Values of C(liq.)/C(initial) greater than 1 indicate enrichment in the derived liquid and values less than 1 indicate depletion. Reference to the summary chemical enrichment diagram (Fig. 10) indicates that the theoretical trace element model must allow Rb, K, Ni, and Cr to increase while Sr and P decrease in the derived magmas. The model (Fig. 11) involves removal of abundant plagioclase, minor olivine, and trace apatite. If during 6-8% fractionation more than 15 to 20% olivine is removed, the Ni and Cr values rapidly reverse directions and become depleted in the evolving magmas. Similarly, rapid depletion of Ni and Cr develops when significant amounts of orthopyroxene or magnetite are removed. Therefore, to support the observed Ice Springs trends of inter- and intra-eruption variations of increasing Rb, Ni, and Cr, plagioclase must be the dominant fractionating phase. Removal of minor amounts of apatite is also necessary to deplete the derived magma in phosphorus.

An independent estimate of the degree of fractionation can be calculated from the Zr data. If the distribution coefficient of Zr in all fractionation phases is assumed to be nearly zero, then an estimate of the percent fractionation is simply the ratio of the initial concentration to the derived concentration of Zr. For the Ice Springs inter-eruption variations, a value of 7% fractionation based on the Zr data agrees well with the 6-8% estimates of the major element fractionation models. For the intra-eruption variations, the Zr data indicates little or no significant fractionation within the limits of Zr analysis. This conflict between the major element and trace element

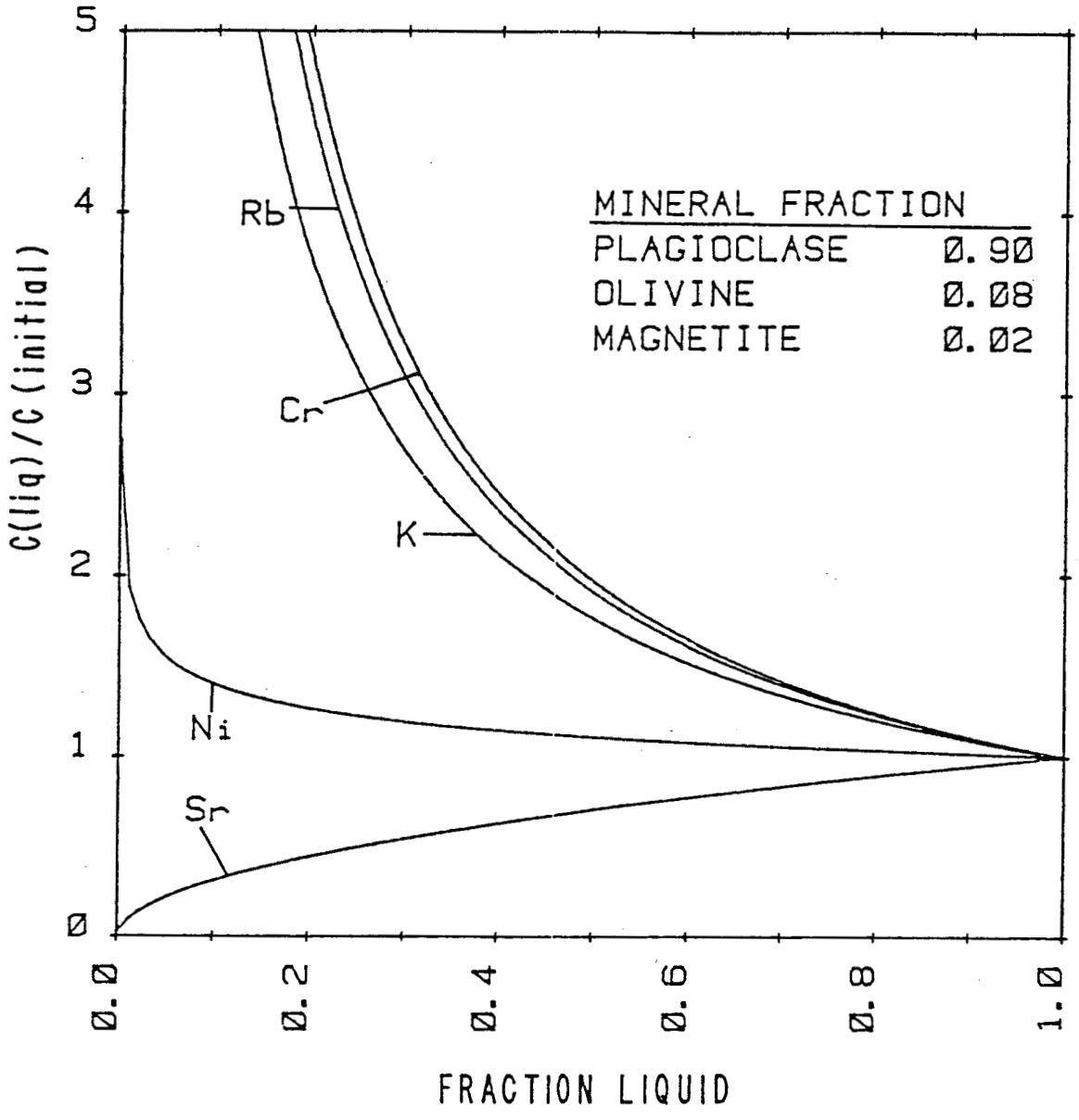


Figure 11. Trace element model for Ice Springs basalts assuming Rayleigh fractionation in terms of Concentration in derived liquid/ concentration in original liquid versus percent solid.

models and also the difference in the importance of the Ni-Cr depleting phases such as olivine, orthopyroxene, and magnetite warrants consideration of additional processes for development of differentiation in the Ice Springs basalts.

Assimilation of large amounts of crustal country rocks of silicious composition would have dramatic effects on the composition of basaltic magmas. Major element assimilation processes can be modeled using the addition-subtraction diagrams of Bowen (1928). These calculations indicate that variations in the amounts of assimilation can account for the observed trends between Ice Springs eruptions. Addition of 7% of the xenolithic material (BRD 77-50G) to the Terrace material will create the major element compositions of the Crescent eruptions. However, assimilation of 7% silicious material low in Ni and Cr and high in Zr should create significant changes in the Ni, Cr, Zr, and other trace element data. Specifically, 7% assimilation into Terrace compositional material should increase Zr and decrease Ni and Cr to values of 173, 108, and 192 respectively. However, all three of these elements behave coherently (Fig. 10). Thermal constraints also limit the amount of assimilation which can occur in basaltic magmas and assimilation greater than a few percent is not compatible with thermal considerations (Bowen, 1928). Therefore, although models can be proposed for assimilation and fractionation being the dominant processes acting to create the Ice Springs trends, the trace element data are not completely consistent with any simple models.

Isotopic Evidence

The Sr isotopic data of Puskar and Condie (1973) shows systematic inter-eruption increases from the oldest Crescent material (87Sr/86Sr = 0.7052) to the youngest Terrace material (87Sr/86Sr = 0.7059). They qualitatively interpreted this trend as the result of mixing magmas having different fractionation and assimilation histories. These conclusions were based on a simple hyperbolic mixing model as clarified by Faure (1977). Quantification of their model in light of the known magma compositions of the Black Rock Desert was unsuccessful as shown in Figure 12. Figure 12 shows the simple hyperbolic end member mixing of the most primitive Black Rock Desert magma (87Sr/86Sr = 0.7044) with the most evolved derived magmas of the Tabernacle (875r/865r = 0.7055) and Pavant (875r/86Sr = 0.7057) volcanic fields of the Black Rock Desert. The observed compositions of the Ice Springs trend is beyond the limits of simple mixing unless magmas of unusual composition are called upon. The simple hyperbolic mixing model cannot account for the isotopic variations of the Ice Springs basalts.

Taylor et al. (1980) in his work on the Roman Comagmatic region of Italy considered the systematic variations in Sr isotopes to be the result of a differentiation process involving concurrent fractional crystallization and assimilation. Graphical application of his model to the Ice Springs data is shown in Figure 13. The curves represent calculated changes in isotopic composition of the magma as a result of crystallization. The crystallization process affects the isotopic composition because crystallization is considered to result from coupled fractionation and assimilation. The model assumes that

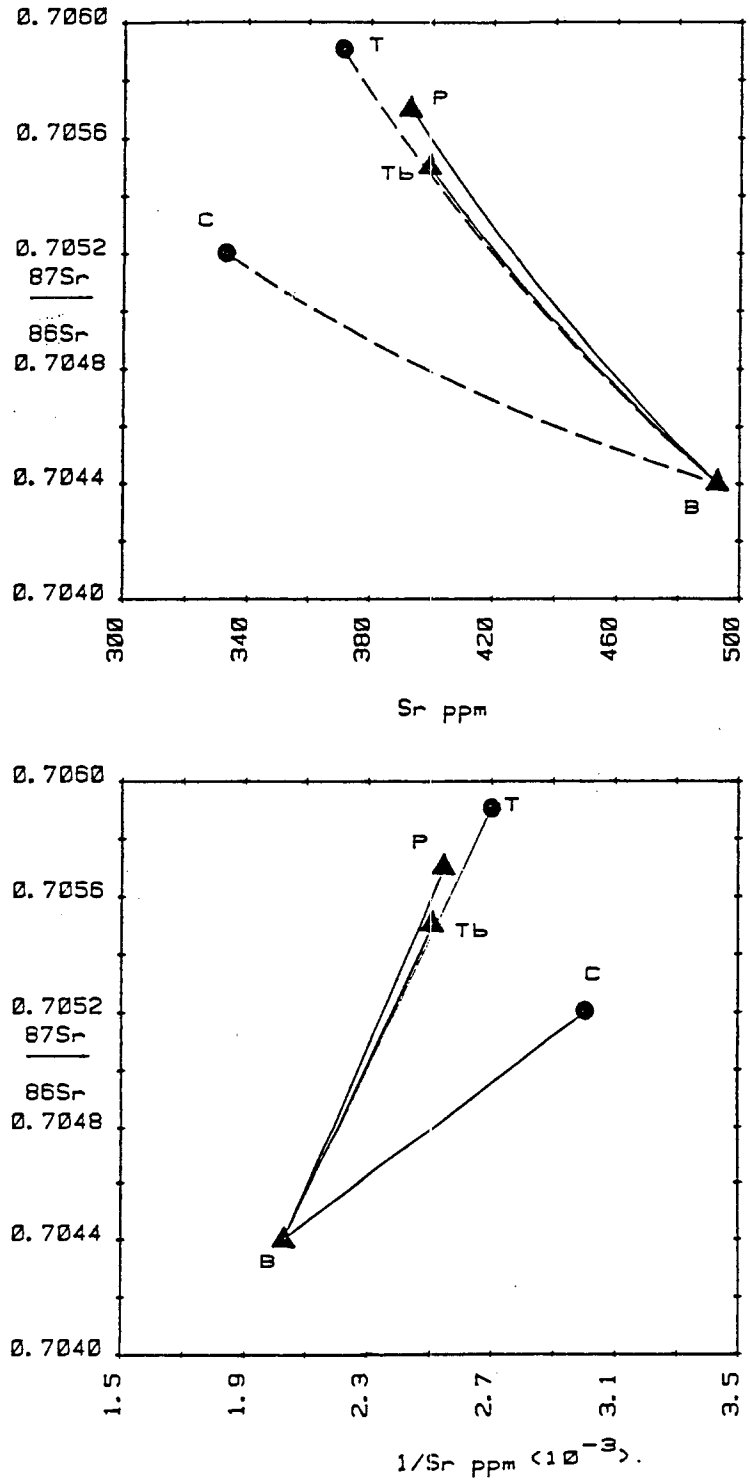


Figure 12. Hyperbolic mixing model for strontium isotope data plotted in terms of 87Sr/86Sr versus Sr ppm (from Faure, 1977).

Figure 13. Combined fractionation and assimilation model for strontium isotope data calculated as by Taylor (1980).

$$87Sr/86Sr_{magma}\ (1 - X_{xtal} + X_{xeno}) = 87Sr/86Sr_{xeno}X_{xeno} + 87Sr/86Sr_{xtal}(1-Xxtal)$$

where:

| | | |
|---|---|---|
| $87Sr/86Sr$ | = | Sr isotopic ratio |
| $X_{xtals}$ | = | Fraction of crystal removed |
| $X_{xeno}$ | = | Fraction of xenolith assimilated |
| $87Sr/86Sr_{xtal}$ | = | Sr isotopic ratio of crystals removed |
| $87Sr/86Sr_{xeno}$ | = | Sr isotopic ratio of assimilated xenoliths |

For thermal balance:

$$\Delta T_m C_{xeno}(X_{xtal}) + L_{xeno}(X_{xeno}) = L_{xtal}(X_{xtal})$$

or $$X_{xeno}/X_{xtal} = L_{xeno}/(\Delta T_m C_{xeno} + L_{xtal}) = k$$

Substitution yields:

$$87Sr/86Sr_{magma} = SR87/Sr86_{xtal} + (87Sr/86Sr_{xeno}k - 87Sr/86Sr_{xtal})F\ /\ (1 + (k-1)F$$

where F = fraction of magma crystallized.

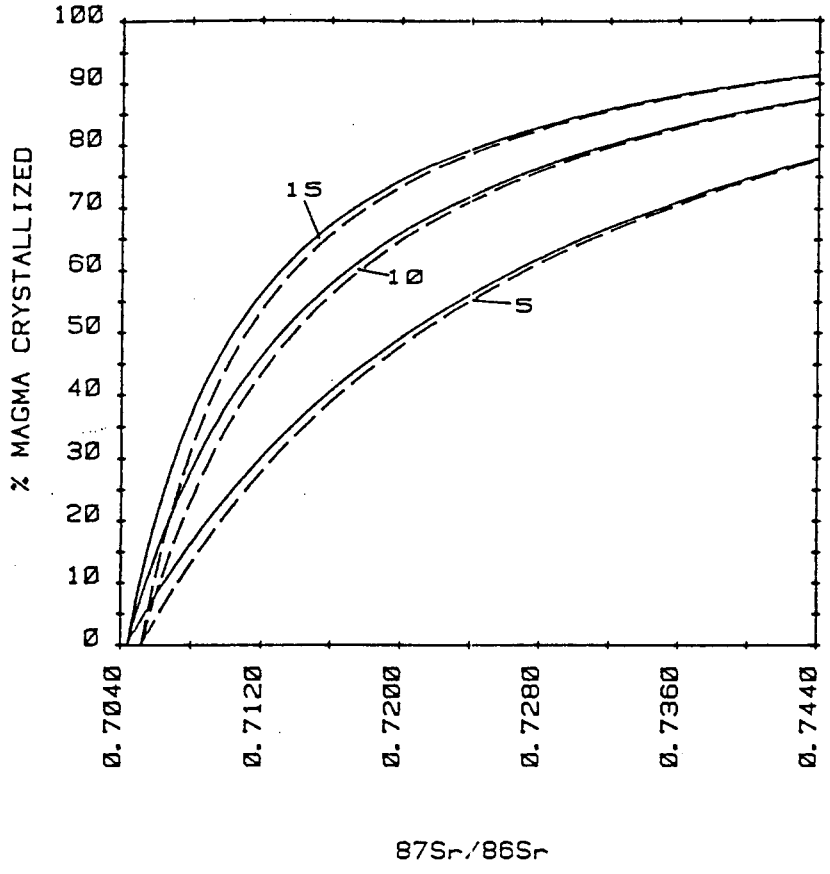
100
90
80
70
60
50
40
30
20
10
0
% MAGMA CRYSTALLIZED
15
10
5
0.7040
0.7120
0.7200
0.7280
0.7360
0.7440
87Sr/86Sr

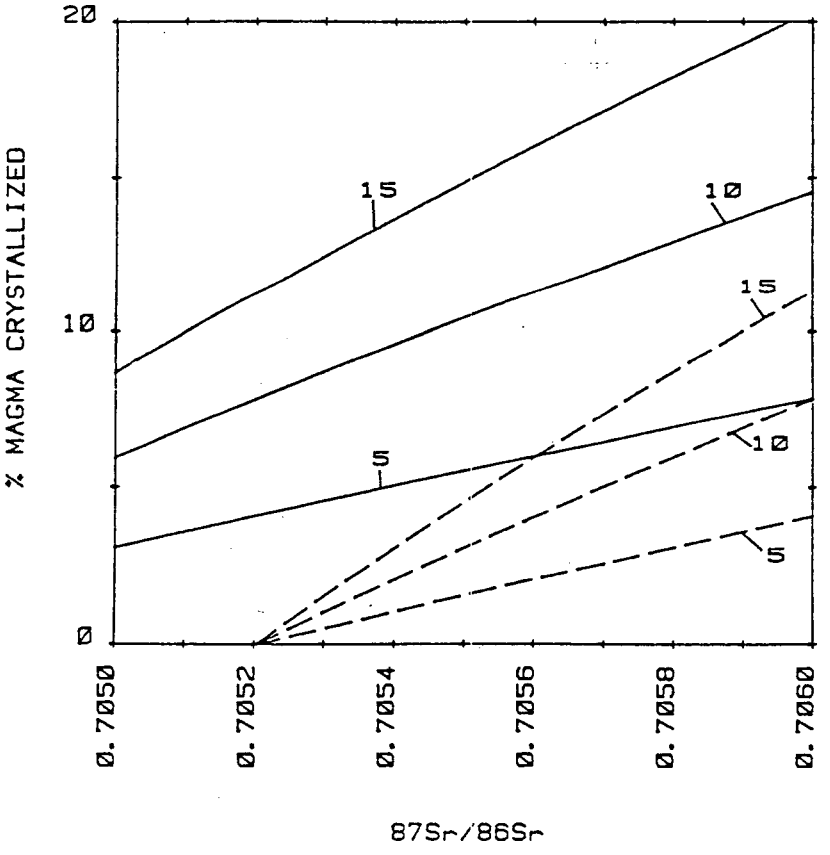
20
10
0
% MAGMA CRYSTALLIZED
15
10
15
5
10
5
0.7050
0.7052
0.7054
0.7056
0.7058
0.7060
87Sr/86Sr

fractionation and assimilation thermally balance each other and result from end member mixing of magma and xenoliths. The end members used in the calculations are from Puskar and Condie (1973) and include the most primitive Black Rock Desert basalt with 87Sr/86Sr of 0.7044 and crustal granitic xenoliths approximately 1.7 b.y. age with 87Sr/86Sr of 0.8000. The series of curves for these end members represent varying the proportions of material assimilated to the amount of crystals fractionated. The thermal constraints of the assimilation process indicate that the ratio of assimilated material to fractionated material is likely to be between 1:5 and 1:15 (Taylor et. al., 1980). If assimilation and fractionation processes are operating together for the Ice Springs basalts, the isotopic variation of the eruptions can be explained by varying the ratios of assimilated material to fractionated crystals or by increasing the percentage of magma crystallized. The whole rock chemical data shows trends of increasing fractionation with decreasing isotopic ratios. Therefore, the direction of evolution is seen as increasing the percentage of magma crystallized while decreasing the ratio of material assimilated to create the Crescent material from the Terrace. For this ideal case, these results imply that a 5 to 8% difference in the amount of fractionation linked with similar amounts of assimilation must exist between the Terrace and Crescent eruptions. If the processes of assimilation and fractionation are not coupled as envisioned by the ideal case, or if only isotopic assimilation is assumed to occur, then the isotopic variations of the Ice Springs basalts would be more compatible with the trace element and the major element data. Specifically, by fractionating approximately

5% and assimilating approximately 1%, the isotopic trends of increasing Sr87/Sr86 and the trace element and major element trends from early to late eruptions in the Ice Springs field might be explained. However, quantification of this uncoupled process is difficult to confirm.

As an additional isotopic constraint, potassium-argon dating was performed to investigate the importance of assimilation. Material analyzed included basaltic cinder glass, basaltic cinder glass adjacent to a silicious inclusion, basaltic lava from a distal flow, and also a silicious inclusion from a cinder cone. All samples of the Holocene Ice Springs basalts contain excess argon as listed in Table 13. This observation is confirmed by the calculated "ages" of the basalts which range from 4 to 16 million years. The actual age of the Ice Springs basalts based on Carbon-14 dating (Valastro, 1972) and geomorphic evidence (Hoover, 1974) is 600 years. Excess radiogenic argon has been reported in 3 basaltic lavas by Dalrymple (1969) with excess argon ranging from .025 to 1.02 ($10^{-11}$ moles/gram). The Ice Springs values of .3 to .08 ($10^{-11}$ moles/gram) are large and indicate that significant outgassing or assimilation of high radiogenic argon containing material must have occurred. Two possible sources of the excess argon are the megacrysts of orthopyroxene and the old silicious inclusions. The excess argon can be accounted for by assimilation of a minimum of 0.05 to 0.1% of 1.85 billion year old granitic inclusions similar to crustal material in northern Utah (Hedge, 1980). This value is a minimum because the hot basalt is likely to have degassed excess argon as eruption occurred. Degassing of the basalt is noted by the decrease in excess argon from the vent related cinders to the distal flows. If

Table 13. Potassium-Argon Analyses of the Ice Springs Basalts.

| Sample Type | Excess $^{40}Ar$ ($10^{-12}$ moles/gram) | Approximate Calculated "AGE" m.y. |
|---|---|---|
| Basaltic cinder glass | 3.005 | 16 |
| Basaltic cinder glass adjacent to a silicious inclusion. | 1.862 | 9.9 |
| Basaltic lava 3 km from vent | .892 | 4.3 |
| Silicious inclusion in cinder | 66.3 | 27.5 |

similar degassing took place during eruption, the quantity of material needed to create the excess argon of the basalts would be greater. The lack of significant quantities of orthopyroxene and the availability of the silicious inclusions indicates that outgassing and assimilation of the silicious inclusions is the source of the excess argon. However, the volume of assimilation predicted by this quantity of excess argon is likely to have been less than 1% and as such would have had little effect on the overall chemical composition of the Ice Springs basalts.

## SUMMARY

The Ice Springs basalts display systematic, consistent, and significant trends in major element, trace element, and isotopic compositions. A reasonable model for the development of the inter- and intra-eruption chemical variations must combine several processes of magmatic differentiation. The model allows for the initial generation of magma by approximately 20% partial melting of lherzolite. Modification of these initial melts results from deep magmatic fractionation of 17 to 20% olivine. The presence of orthopyroxene megacrysts suggests a role for deep pyroxene fractionation. However, the lack of a pyroxene related Sc depletion and the compatibility of the magnesium number and trace element fractionation calculations indicates that olivine was the dominant initial fractionating phase. After the deep modification, magma pulses moved upward through the crust and arrived in shallow level staging chambers as modified melts. Subsequent contamination by less than 1% assimilation of crustal material and differentiation by 3 to 8% fractional crystallization of plagioclase, olivine, and a magnetite additionally modified the chemical character of the magmas. The final chemical trends shown in the Ice Springs lavas and cinders likely resulted as slightly different composition magmas mixed in the shallow staging chamber and erupted onto the surface.

The systematic chemical variations during eruptions of the Ice

Springs basalts limit the importance of the processes of magmatic differentiation. Specifically, the role of shallow fractionation as a differentiation process is supported by the observed textural and chemical relations. The presence of zoned plagioclase xenocrysts and the lack of early formed olivine phenocrysts suggests that plagioclase played the dominant role in crystal fractionation. Also, the lack of Ni, Cr, and Rb depletions and the observed Sr depletions in the derived magmas supports the importance of 6 to 8% fractionation of plagioclase with minor olivine and magnetite involvement from Terrace to Crescent eruptions. The chemical data also limits assimilation to less than 1% of silicious crustal material. The effects of larger amounts of assimilation would be dramatically different than the observed chemical trends.

The overall chemical trends agree well with the textural and chemical evidence supporting the processes of assimilation and fractionation. However, the additional complication of interaction of slightly different composition magmas in a shallow staging chamber can also help explain the Ice Springs trends. The importance of small scale mixing of magmas is difficult to test because of the unknown nature of the end members magmas. But, the interaction of two similar magmas is a process which could initiate an eruptive event by increasing shallow magmatic pressures and which could also create the rapid chemical trends over the evolution of an individual cinder cone and the whole volcanic field. The consistency of the chemical trends over time implies coherence and consistency of the differentiation processes over time. The possibility that random mixing of magmas

created the systematic chemical trends over time seems unlikely. Therefore, the systematic chemical trends developed in the Ice Springs eruptive sequence suggests that differentiation results from a complex interplay of fractionation, assimilation, and minor magma interaction.

Appendix 1. Basic chemical data for the Ice Springs basalts with group classifications and relative plotting elevations for all data. $Fe_2O_3(T)$ is total iron reported as $Fe_2O_3$ and recalculated $Fe_2O_3$ and FeO values are based on BRD77-12 oxidation ratio.

LATE CRESCENT

| Wt.% | BRD1.0 | BRD1.7 | BRD2.5 | BRD3.3 | BRD4.8 | BRD6.2 | BRD7.6 | BRD8.5 | BRD9.5 | BRD10.3 | BRD11.0 | BRD12 |
|---|---|---|---|---|---|---|---|---|---|---|---|---|
| $SiO_2$ | 50.33 | 50.84 | 49.96 | 51.04 | 51.95 | 51.92 | 51.53 | 50.28 | 51.03 | 50.90 | 51.52 | 52.17 |
| $TiO_2$ | 1.76 | 1.76 | 1.76 | 1.77 | 1.78 | 1.82 | 1.78 | 1.75 | 1.79 | 1.72 | 1.73 | 1.70 |
| $Al_2O_3$ | 15.78 | 15.57 | 15.15 | 15.38 | 15.61 | 15.48 | 14.67 | 15.35 | 15.54 | 15.52 | 15.43 | 15.43 |
| $Fe_2O_3$(T) | 10.95 | 11.17 | 11.05 | 11.15 | 11.18 | 11.25 | 11.18 | 10.98 | 11.19 | 10.93 | 10.89 | 10.83 |
| MnO | 0.18 | 0.18 | 0.19 | 0.18 | 0.19 | 0.19 | 0.19 | 0.18 | 0.19 | 0.18 | 0.18 | 0.17 |
| MgO | 7.45 | 7.60 | 7.43 | 7.49 | 7.29 | 7.35 | 7.18 | 7.24 | 7.43 | 7.13 | 7.66 | 7.19 |
| CaO | 8.94 | 9.11 | 8.88 | 9.01 | 9.00 | 9.11 | 8.98 | 8.80 | 8.81 | 8.57 | 8.95 | 8.75 |
| $K_2O$ | 1.20 | 1.23 | 1.18 | 1.21 | 1.24 | 1.24 | 1.25 | 1.26 | 1.26 | 1.36 | 1.31 | 1.38 |
| $Na_2O$ | 2.96 | 2.95 | 2.72 | 2.84 | 3.18 | 2.99 | 3.08 | 3.24 | 2.74 | 2.55 | 3.13 | 3.29 |
| $P_2O_5$ | 0.54 | 0.56 | 0.50 | 0.52 | 0.55 | 0.55 | 0.50 | 0.54 | 0.55 | 0.53 | 0.48 | 0.52 |
| Loss | 0.12 | 0.50 | 0.23 | 0.00 | 0.37 | 0.35 | 0.53 | 0.00 | 0.80 | 0.95 | 0.00 | 0.06 |
| Total | 100.20 | 101.47 | 99.05 | 100.59 | 102.34 | 102.25 | 100.87 | 99.62 | 101.33 | 100.35 | 101.28 | 101.49 |
| FeO | 8.71 | 8.89 | 8.79 | 8.87 | 8.89 | 8.95 | 8.89 | 8.73 | 8.90 | 8.69 | 8.66 | 8.62 |
| $Fe_2O_3$ | 1.27 | 1.29 | 1.28 | 1.29 | 1.30 | 1.30 | 1.30 | 1.27 | 1.30 | 1.27 | 1.26 | 1.26 |
| Nb* | 20 | 19 | 19 | 20 | 19 | 21 | 24 | 19 | 19 | 23 | 20 | 19 |
| Zr* | 175 | 173 | 173 | 177 | 177 | 151 | 157 | 157 | 156 | 166 | 156 | 165 |
| Y* | 28 | 29 | 29 | 33 | 32 | 30 | 31 | 31 | 30 | 30 | 30 | 32 |
| Sr* | 363 | 366 | 366 | 366 | 363 | 344 | 348 | 354 | 352 | 341 | 335 | 344 |
| Rb* | 22 | 24 | 23 | 24 | 24 | 21 | 21 | 22 | 23 | 24 | 25 | 30 |
| Th* | 3 | 0 | 0 | 2 | 6 | 1 | 1 | 0 | 0 | 1 | 5 | 8 |
| Ni* | 133 | - | - | - | - | - | - | - | - | - | 129 | - |
| Cr* | 246 | - | - | - | - | - | - | - | - | - | 251 | - |
| Elev. | 401 | 402 | 403 | 404 | 405 | 406 | 407 | 408 | 409 | 410 | 411 | 412 |

*weight expressed in parts per million (ppm)

EARLY CRESCENT

| Wt.% | BRD13 | BRD14 | BRD15 | BRD16 | BRD17 | BRD18 | BRD19 | BRD20.4 | BRD22 | BRD23 | BRD24 | BRD25 |
|---|---|---|---|---|---|---|---|---|---|---|---|---|
| $SiO_2$ | 53.07 | 52.68 | 51.49 | 52.09 | 51.35 | 52.64 | 52.46 | 52.69 | 52.01 | 51.82 | 52.57 | 50.11 |
| $TiO_2$ | 1.65 | 1.60 | 1.55 | 1.58 | 1.55 | 1.52 | 1.58 | 1.61 | 1.57 | 1.52 | 1.52 | 1.54 |
| $Al_2O_3$ | 15.63 | 15.52 | 15.63 | 15.63 | 15.47 | 15.74 | 16.00 | 15.96 | 16.22 | 15.34 | 15.18 | 14.55 |
| $Fe_2O_3$(T) | 10.56 | 10.33 | 10.08 | 10.27 | 10.21 | 10.22 | 10.16 | 10.27 | 10.20 | 9.77 | 9.91 | 9.90 |
| MnO | 0.18 | 0.17 | 0.16 | 0.16 | 0.16 | 0.16 | .16 | .17 | .16 | .16 | .16 | .17 |
| MgO | 7.32 | 7.46 | 7.37 | 7.30 | 7.47 | 7.50 | 7.36 | 7.72 | 7.17 | 7.36 | 7.42 | 6.79 |
| CaO | 8.70 | 8.78 | 8.61 | 8.59 | 8.51 | 8.75 | 8.74 | 8.95 | 8.93 | 8.52 | 8.63 | 8.40 |
| $K_2O$ | 1.50 | 1.50 | 1.47 | 1.48 | 1.46 | 1.47 | 1.48 | 1.49 | 1.46 | 1.46 | 1.51 | 1.44 |
| $Na_2O$ | 3.18 | 2.94 | 3.33 | 2.92 | 3.17 | 3.28 | 3.51 | 3.35 | 3.18 | 2.59 | 2.67 | 2.28 |
| $P_2O_5$ | 0.49 | 0.46 | 0.48 | 0.46 | 0.47 | 0.48 | .49 | .45 | .48 | .45 | .46 | .47 |
| Loss | 0.05 | 0.13 | 0.34 | 0.34 | 0.15 | 0.27 | .49 | .62 | .31 | .60 | .63 | .40 |
| Total | 102.33 | 101.57 | 100.82 | 100.82 | 99.97 | 102.09 | 102.43 | 103.28 | 101.69 | 98.99 | 100.03 | 96.05 |
| FeO | 8.40 | 8.22 | 8.02 | 8.17 | 8.12 | 8.13 | 8.08 | 8.17 | 8.11 | 7.77 | 7.88 | 7.87 |
| $Fe_2O_3$ | 1.22 | 1.20 | 1.17 | 1.19 | 1.18 | 1.18 | 1.18 | 1.19 | 1.18 | 1.13 | 1.15 | 1.15 |
| Nb* | 18 | 19 | 18 | 20 | 20 | 24 | 24 | 24 | 21 | 22 | 23 | 23 |
| Zr* | 167 | 169 | 167 | 160 | 165 | 165 | 165 | 165 | 158 | 164 | 164 | 167 |
| Y* | 31 | 31 | 30 | 26 | 26 | 28 | 28 | 28 | 27 | 29 | 27 | 28 |
| Sr* | 335 | 341 | 345 | 328 | 334 | 332 | 340 | 336 | 335 | 340 | 339 | 345 |
| Rb* | 30 | 35 | 34 | 29 | 31 | 29 | 30 | 29 | 31 | 33 | 33 | 35 |
| Th* | 8 | 10 | 14 | 0 | 0 | 2 | 6 | 0 | 7 | 7 | 9 | 10 |
| Ni* | - | - | - | - | - | - | - | - | 148 | - | - | - |
| Cr* | - | - | - | - | - | - | - | - | 270 | - | - | - |
| Elev. | 413 | 414 | 415 | 416 | 417 | 418 | 419 | 420 | 422 | 423 | 424 | 425 |

*Weight, expressed in parts per million (ppm)

| | EARLY CRESCENT | | | | FLOW CRESCENT | | | | LATE TERRACE | | | |
|---|---|---|---|---|---|---|---|---|---|---|---|---|
| Wt.% | BRD26 | BRD27 | BRD29 | BRD30 | ISB-03 | ISB-4 | ISB-7 | ISB-13 | ISB-14 | ISB-15 | ISB-16 | ISB-17 |
| $SiO_2$ | 52.42 | 52.55 | 52.94 | 52.26 | 49.79 | 49.87 | 44.36 | 50.22 | 49.90 | 50.77 | 49.81 | 48.58 |
| $TiO_2$ | 1.55 | 1.55 | 1.56 | 1.53 | 1.77 | 1.78 | 1.30 | 1.91 | 1.97 | 1.97 | 1.94 | 1.91 |
| $Al_2O_3$ | 15.97 | 15.89 | 15.76 | 14.81 | 15.48 | 15.29 | 3.54 | 15.08 | 15.20 | 15.14 | 14.76 | 14.88 |
| $Fe_2O_3$(T) | 9.98 | 10.01 | 10.07 | 9.91 | 11.07 | 10.95 | 8.46 | 11.26 | 11.50 | 11.59 | 11.50 | 11.30 |
| MnO | .16 | .17 | .17 | .16 | .18 | .18 | .15 | .18 | .19 | .19 | .19 | .18 |
| MgO | 7.46 | 7.35 | 7.71 | 7.53 | 8.18 | 7.11 | 6.78 | 6.93 | 6.67 | 6.97 | 6.37 | 6.93 |
| CaO | 8.78 | 8.72 | 8.94 | 8.82 | 8.77 | 8.96 | 7.88 | 9.04 | 8.66 | 8.78 | 8.79 | 8.64 |
| $K_2O$ | 1.44 | 1.44 | 1.46 | 1.44 | 1.24 | 1.23 | 1.31 | 1.23 | 1.31 | 1.28 | 1.31 | 1.19 |
| $Na_2O$ | 2.65 | 2.87 | 2.51 | 2.37 | 2.79 | 3.16 | 2.44 | 2.69 | 2.72 | 2.70 | 1.88 | 2.63 |
| $P_2O_5$ | .44 | .48 | .48 | .46 | .47 | .55 | .36 | .61 | .59 | .60 | .57 | .56 |
| Loss | .24 | .40 | .26 | .66 | .21 | 2.27 | 5.41 | 1.10 | .59 | .48 | .10 | .61 |
| Total | 100.85 | 101.43 | 101.86 | 100.07 | 99.95 | 101.36 | 91.98 | 100.25 | 99.30 | 100.48 | 97.21 | 97.41 |
| FeO | 7.94 | 7.96 | 8.01 | 7.88 | 8.82 | 8.71 | 6.72 | 8.96 | 9.14 | 9.21 | 9.14 | 8.98 |
| $Fe_2O_3$ | 1.16 | 1.16 | 1.17 | 1.15 | 1.29 | 1.27 | .98 | 1.31 | 1.33 | 1.34 | 1.33 | 1.31 |
| Nb* | 24 | 20 | 21 | 21 | 21 | 20 | 21 | 20 | 19 | 23 | 20 | 19 |
| Zr* | 164 | 155 | 160 | 161 | 146 | 154 | 157 | 163 | 172 | 171 | 168 | 163 |
| Y* | 29 | 27 | 27 | 28 | 28 | 30 | 29 | 32 | 32 | 34 | 32 | 29 |
| Sr* | 351 | 334 | 341 | 342 | 345 | 352 | 336 | 363 | 366 | 372 | 351 | 375 |
| Rb* | 33 | 30 | 30 | 32 | 24 | 24 | 32 | 25 | 24 | 23 | 22 | 23 |
| Th* | 9 | 9 | 6 | 4 | 4 | 7 | 3 | 5 | 5 | 2 | 5 | 4 |
| Ni* | - | - | - | 146 | 126 | - | - | - | - | - | - | - |
| Cr* | - | - | - | 273 | 230 | - | - | - | - | - | - | - |
| Elev. | 426 | 427 | 429 | 430 | 400 | 400 | 400 | 100 | 101 | 102 | 103 | 104 |

*Weight expressed in parts per million (ppm)

| | LATE TERRACE | | | | | EARLY TERRACE | | | | | | |
|---|---|---|---|---|---|---|---|---|---|---|---|---|
| Wt.% | ISB-18 | ISB-19 | ISB-20 | ISB-21 | ISB-22 | ISB-23 | ISB-24 | ISB-25 | ISB-26 | ISB-27 | ISB-28 | ISB-29 |
| $SiO_2$ | 49.93 | 50.73 | 50.20 | 50.79 | 50.10 | 49.23 | 47.78 | 48.88 | 48.50 | 51.33 | 50.11 | 49.14 |
| $TiO_2$ | 1.87 | 1.92 | 1.90 | 1.92 | 1.90 | 1.79 | 1.88 | 1.86 | 1.90 | 1.95 | 1.92 | 1.83 |
| $Al_2O_3$ | 14.78 | 15.49 | 14.95 | 15.09 | 15.31 | 14.80 | 14.94 | 15.16 | 15.16 | 15.87 | 15.78 | 15.25 |
| $Fe_2O_3$(T) | 11.24 | 11.39 | 11.17 | 11.56 | 11.59 | 10.96 | 11.31 | 11.14 | 11.35 | 11.85 | 11.60 | 11.34 |
| MnO | .19 | .18 | .18 | .19 | .19 | .19 | .19 | .18 | .19 | .20 | .19 | .18 |
| MgO | 7.02 | 6.96 | 6.96 | 7.27 | 7.27 | 7.16 | 7.61 | 7.45 | 7.62 | 7.63 | 7.51 | 7.67 |
| CaO | 8.88 | 8.94 | 9.30 | 9.12 | 9.44 | 8.81 | 9.37 | 9.53 | 9.53 | 8.33 | 9.38 | 9.32 |
| $K_2O$ | 1.19 | 1.23 | 1.22 | 1.12 | 1.06 | 1.10 | .95 | .98 | .99 | .99 | 1.03 | 1.02 |
| $Na_2O$ | 2.53 | 3.10 | 3.03 | 2.63 | 2.85 | 2.55 | 3.01 | 2.53 | 3.20 | 2.71 | 2.97 | 2.59 |
| $P_2O_5$ | .58 | .59 | .59 | .59 | .58 | .51 | .53 | .53 | .53 | .53 | .54 | .52 |
| Loss | .76 | .68 | 1.16 | .69 | .83 | 1.30 | .57 | 1.13 | .87 | .78 | .74 | 1.13 |
| Total | 98.97 | 101.20 | 100.66 | 100.96 | 101.11 | 98.40 | 98.14 | 99.37 | 99.84 | 102.16 | 101.77 | 99.98 |
| FeO | 8.93 | 9.05 | 8.82 | 9.19 | 9.21 | 8.71 | 8.99 | 8.85 | 9.02 | 9.42 | 9.22 | 9.02 |
| $Fe_2O_3$ | 1.30 | 1.39 | 1.89 | 1.34 | 1.34 | 1.27 | 1.31 | 1.29 | 1.31 | 1.37 | 1.34 | 1.31 |
| Nb* | 19 | 19 | 19 | 20 | 21 | 20 | 19 | 20 | 21 | 22 | 21 | 21 |
| Zr* | 165 | 163 | 155 | 152 | 144 | 142 | 136 | 138 | 133 | 140 | 138 | 142 |
| Y* | 30 | 29 | 29 | 31 | 30 | 29 | 29 | 30 | 29 | 29 | 29 | 30 |
| Sr* | 379 | 377 | 372 | 361 | 377 | 353 | 394 | 399 | 368 | 346 | 376 | 379 |
| Rb* | 25 | 24 | 23 | 21 | 21 | 27 | 18 | 21 | 19 | 20 | 20 | 22 |
| Th* | 9 | 5 | 3 | 6 | 7 | 3 | 4 | 6 | 6 | 0 | 0 | 3 |
| Ni* | 108 | - | - | - | - | - | - | - | - | - | - | - |
| Cr* | 190 | - | - | - | - | - | - | - | - | - | - | - |
| Elev. | 105 | 106 | 107 | 108 | 109 | 110 | 111 | 113 | 114 | 116 | 118 | 120 |

*weight expressed in parts per million (ppm)

| | EARLY TERRACE | | | FLOW TERRACE | | | | MITER | | | | |
|---|---|---|---|---|---|---|---|---|---|---|---|---|
| Wt.% | ISB-30 | ISB-31 | ISB-32 | ISB-83 | ISB-84 | ISB-85 | ISB-92 | ISB-52 | ISB-53 | ISB-54 | ISB-55 | ISB-56 |
| $SiO_2$ | 49.06 | 48.72 | 49.35 | 51.11 | 49.47 | 49.02 | 49.06 | 53.01 | 50.10 | 50.85 | 47.85 | 50.97 |
| $TiO_2$ | 1.81 | 1.86 | 1.85 | 1.96 | 1.84 | 1.91 | 1.90 | 1.46 | 1.97 | 2.00 | 1.89 | 1.99 |
| $Al_2O_3$ | 15.19 | 15.38 | 15.46 | 15.90 | 15.88 | 15.59 | 15.27 | 15.66 | 15.32 | 15.68 | 14.16 | 15.62 |
| $Fe_2O_3$(T) | 11.22 | 11.70 | 11.51 | 11.99 | 11.73 | 11.67 | 11.68 | 10.00 | 11.77 | 12.02 | 11.42 | 11.94 |
| MnO | .18 | .18 | .19 | .19 | .19 | .18 | .19 | .16 | .18 | .19 | .19 | .18 |
| MgO | 7.53 | 7.52 | 7.41 | 8.03 | 8.69 | 8.68 | 7.20 | 7.53 | 7.09 | 7.18 | 6.13 | 7.47 |
| CaO | 9.53 | 9.41 | 9.59 | 8.91 | 9.10 | 9.04 | 8.76 | 8.96 | 8.41 | 8.81 | 8.26 | 8.77 |
| $K_2O$ | 1.09 | 1.05 | 1.04 | 1.29 | 1.09 | .96 | 1.19 | 1.52 | 1.17 | 1.16 | 1.16 | 1.15 |
| $Na_2O$ | 2.77 | 3.27 | 2.89 | 2.92 | 2.92 | 3.35 | 3.05 | 3.05 | 3.07 | 2.94 | 2.28 | 2.69 |
| $P_2O_5$ | .54 | .52 | .55 | .54 | .51 | .55 | .56 | .38 | .56 | .60 | .54 | .57 |
| Loss | 1.80 | .17 | 1.53 | .00 | .00 | .12 | .00 | .00 | .63 | .00 | 4.02 | 1.69 |
| Total | 100.73 | 99.78 | 101.37 | 102.84 | 101.42 | 101.08 | 98.88 | 101.72 | 100.27 | 101.43 | 97.88 | 103.03 |
| FeO | 8.93 | 9.30 | 9.16 | 9.56 | 9.36 | 9.31 | 9.31 | 8.00 | 9.41 | 9.60 | 9.13 | 9.54 |
| $Fe_2O_3$ | 1.30 | 1.36 | 1.33 | 1.39 | 1.36 | 1.36 | 1.36 | 1.11 | 1.31 | 1.34 | 1.27 | 1.33 |
| Nb* | 19 | 18 | 18 | 20 | 18 | 19 | 24 | 18 | 18 | 18 | 19 | 17 |
| Zr* | 131 | 137 | 143 | 161 | 140 | 138 | 162 | 160 | 159 | 166 | 169 | 164 |
| Y* | 27 | 26 | 27 | 32 | 31 | 28 | 30 | 26 | 30 | 31 | 30 | 28 |
| Sr* | 427 | 366 | 365 | 358 | 376 | 380 | 371 | 346 | 344 | 366 | 347 | 358 |
| Rb* | 22 | 17 | 23 | 21 | 19 | 23 | 23 | 29 | 19 | 22 | 22 | 21 |
| Th* | 3 | 5 | 7 | 10 | 10 | 10 | 11 | 3 | 3 | 12 | 6 | 10 |
| Ni* | - | - | - | - | 125 | - | - | - | - | - | - | - |
| Cr* | - | - | - | - | 220 | - | - | - | - | - | - | - |
| Elev. | 122 | 124 | 126 | 100 | 100 | 100 | 100 | 300 | 301 | 303 | 305 | 307 |

*Weight expressed in parts per million (ppm)

| | MITER | | | | | | | | FLOW MITER | | |
|---|---|---|---|---|---|---|---|---|---|---|---|
| Wt.% | ISB-57 | ISB-58 | ISB-59 | ISB-60 | ISB-61 | ISB-62-A | ISB-62-B | ISB-63 | ISB-64 | ISB-42 | ISB-43 | ISB-91 |
| $SiO_2$ | 50.59 | 47.76 | 49.50 | 51.05 | 49.96 | 50.70 | 49.50 | 51.34 | 51.41 | 51.50 | 47.25 | 49.03 |
| $TiO_2$ | 1.97 | 1.93 | 1.90 | 1.95 | 1.90 | 1.93 | 1.75 | 1.73 | 2.02 | 1.40 | 1.88 | 1.92 |
| $Al_2O_3$ | 15.38 | 15.36 | 15.24 | 15.32 | 15.23 | 16.10 | 14.95 | 15.48 | 15.59 | 16.00 | 15.09 | 14.87 |
| $Fe_2O_3$(T) | 11.92 | 11.87 | 11.62 | 11.77 | 11.62 | 11.79 | 11.01 | 10.85 | 12.10 | 9.65 | 11.31 | 11.86 |
| MnO | .19 | .19 | .18 | .18 | .18 | .18 | .17 | .18 | .19 | .16 | .19 | .18 |
| MgO | 7.21 | 6.97 | 7.24 | 7.38 | 7.21 | 7.73 | 6.95 | 7.37 | 7.29 | 8.54 | 7.58 | 7.31 |
| CaO | 8.70 | 8.62 | 8.55 | 9.10 | 9.06 | 9.23 | 8.96 | 9.26 | 9.20 | 8.56 | 11.22 | 8.67 |
| $K_2O$ | 1.18 | 1.10 | 1.09 | 1.05 | 1.11 | .95 | 1.21 | 1.38 | 1.17 | 1.51 | 1.03 | 1.18 |
| $Na_2O$ | 3.01 | 3.12 | 3.24 | 3.11 | 3.66 | 2.82 | 2.65 | 2.62 | 2.74 | 2.95 | 2.50 | 3.29 |
| $P_2O_5$ | .60 | .58 | .58 | .60 | .59 | .60 | .54 | .53 | .63 | .37 | .56 | .54 |
| Loss | .16 | .16 | .62 | .73 | .83 | .60 | .98 | 1.29 | .29 | .23 | 2.87 | .00 |
| Total | 100.90 | 97.65 | 99.78 | 102.23 | 101.35 | 102.64 | 98.66 | 102.02 | 102.64 | 100.87 | 101.48 | 98.85 |
| FeO | 9.53 | 9.48 | 9.28 | 9.41 | 9.29 | 9.42 | 8.79 | 8.67 | 9.67 | 7.73 | 9.06 | 9.50 |
| $Fe_2O_3$ | 1.33 | 1.32 | 1.29 | 1.31 | 1.30 | 1.31 | 1.23 | 1.21 | 1.35 | 1.08 | 1.26 | 1.32 |
| Nb* | 19 | 21 | 22 | 22 | 21 | 19 | 20 | 23 | 21 | 22 | 21 | 26 |
| Zr* | 168 | 166 | 173 | 164 | 158 | 149 | 159 | 164 | 164 | 160 | 149 | 162 |
| Y* | 29 | 30 | 32 | 31 | 32 | 27 | 28 | 28 | 30 | 30 | 29 | 31 |
| Sr* | 358 | 346 | 383 | 371 | 376 | 371 | 364 | 368 | 373 | 344 | 366 | 372 |
| Rb* | 20 | 20 | 21 | 20 | 20 | 18 | 24 | 29 | 21 | 34 | 22 | 23 |
| Th* | 7 | 6 | 7 | 0 | 3 | 6 | 6 | 9 | 6 | 11 | 6 | 7 |
| Ni* | - | - | 112 | - | - | - | - | - | - | 142 | - | - |
| Cr* | - | - | 194 | - | - | - | - | - | - | 247 | - | - |
| Elev. | 308 | 310 | 311 | 315 | 317 | 319 | 322 | 324 | 325 | 300 | 300 | 300 |

*Weight expressed in parts per million (ppm)

| | | | | | | | | | | | | |
|---|---|---|---|---|---|---|---|---|---|---|---|---|
| | | | | POCKET | | | | FLOW POCKET | | DISTAL FLOW MATERIAL | | |
| | | | | | | | | | | CRESCENT | | MITER |
| Wt.% | ISB-33 | ISB-34 | ISB-35 | ISB-36 | ISB-37 | ISB-38 | ISB-39 | ISB-40 | ISB-41 | ISB-70 | ISB-80 | ISB-46 |
| $SiO_2$ | 51.51 | 51.83 | 51.27 | 51.54 | 50.98 | 52.01 | 51.54 | 50.56 | 49.29 | 52.73 | 52.30 | 51.70 |
| $TiO_2$ | 1.99 | 1.99 | 1.94 | 1.97 | 1.92 | 1.98 | 1.99 | 1.97 | 1.92 | 1.50 | 1.56 | 1.62 |
| $Al_2O_3$ | 15.48 | 15.50 | 14.85 | 15.10 | 15.29 | 15.43 | 15.37 | 15.61 | 15.26 | 15.75 | 15.45 | 15.19 |
| $Fe_2O_3$ | 11.97 | 11.97 | 11.70 | 11.82 | 11.71 | 11.80 | 11.88 | 11.84 | 11.76 | 10.11 | 10.12 | 10.31 |
| MnO | .19 | .19 | .18 | .18 | .18 | .19 | .18 | .19 | .19 | .18 | .18 | .18 |
| MgO | 7.09 | 6.93 | 6.98 | 6.98 | 7.00 | 7.07 | 7.21 | 7.90 | 7.75 | 7.75 | 7.34 | 6.67 |
| CaO | 8.57 | 8.79 | 8.49 | 8.54 | 8.53 | 8.67 | 8.87 | 8.79 | 8.71 | 8.93 | 9.06 | 8.53 |
| $K_2O$ | 1.28 | 1.37 | 1.27 | 1.32 | 1.29 | 1.28 | 1.17 | 1.25 | 1.26 | 1.42 | 1.51 | 1.42 |
| $Na_2O$ | 2.65 | 3.14 | 3.26 | 3.21 | 3.00 | 2.87 | 2.87 | 2.77 | 2.75 | 2.64 | 3.20 | 2.46 |
| $P_2O_5$ | .56 | .58 | .56 | .55 | .58 | .56 | .57 | .54 | .53 | .45 | .46 | .46 |
| Loss | .37 | .00 | .00 | .00 | .01 | .19 | .35 | .30 | .34 | .01 | .01 | .02 |
| Total | 101.66 | 102.29 | 100.52 | 101.22 | 100.48 | 102.05 | 102.02 | 101.72 | 99.76 | 101.50 | 100.98 | 98.57 |
| Feo | 9.52 | 9.52 | 9.35 | 9.45 | 9.36 | 9.43 | 9.50 | 9.48 | 9.41 | 8.08 | 8.09 | 8.24 |
| $Fe_2O_3$ | 1.39 | 1.39 | 1.30 | 1.32 | 1.31 | 1.32 | 1.32 | 1.32 | 1.31 | 1.13 | 1.13 | 1.15 |
| Nb* | 20 | 22 | 18 | 23 | 18 | 19 | 19 | 21 | 21 | 21 | 21 | 20 |
| Zr* | 174 | 180 | 173 | 172 | 174 | 169 | 164 | 162 | 161 | 153 | 158 | 161 |
| Y* | 31 | 30 | 30 | 31 | 31 | 30 | 29 | 30 | 30 | 26 | 27 | 27 |
| Sr* | 355 | 365 | 360 | 353 | 364 | 360 | 374 | 363 | 364 | 352 | 358 | 333 |
| Rb* | 23 | 25 | 23 | 22 | 23 | 23 | 22 | 24 | 22 | 30 | 28 | 35 |
| Th* | 7 | 7 | 6 | 4 | 4 | 6 | 7 | 6 | 7 | 11 | 7 | 10 |
| Ni* | - | - | 142 | - | - | - | - | 121 | - | - | 131 | - |
| Cr* | - | - | 247 | - | - | - | - | 203 | - | - | 254 | - |
| Elev. | 200 | 201 | 203 | 204 | 205 | 206 | 207 | 200 | 200 | 400 | 400 | 200 |

*Weight expressed in parts per million (ppm)

DISTAL FLOW MATERIAL

| | CRESCENT | | TERRACE | | MITER | TERRACE | INCLUSIONS IN CINDER | | | | |
|---|---|---|---|---|---|---|---|---|---|---|---|
| Wt.% | ISB-99 | ISB-79-B | ISB-90 | ISB-94 | ISB-97 | ISB-102 | 78-50A | 7850-C | 78-50G | 78-50J | ISB-104 |
| $SiO_2$ | 50.57 | 52.30 | 52.53 | 51.55 | 51.52 | 49.55 | 73.42 | 91.28 | 73.56 | 96.68 | 70.14 |
| $TiO_2$ | 1.43 | 1.52 | 1.46 | 1.99 | 1.95 | 1.95 | .01 | .02 | .07 | .02 | .03 |
| $Al_2O_3$ | 14.95 | 15.61 | 15.63 | 15.34 | 15.12 | 14.91 | 13.88 | 4.92 | 14.76 | .70 | 19.54 |
| $Fe_2O_3$ | 9.87 | 9.88 | 9.82 | 12.04 | 11.80 | 12.10 | .00 | .01 | .64 | .00 | .12 |
| MnO | .17 | .17 | .17 | .21 | .20 | .20 | .01 | .01 | .03 | .02 | .02 |
| MgO | 7.07 | 7.30 | 7.22 | 7.17 | 6.78 | 6.59 | .00 | .31 | .39 | .10 | .24 |
| CaO | 8.41 | 7.92 | 8.46 | 9.31 | 8.99 | 9.06 | .50 | .75 | 2.06 | .13 | 3.36 |
| $K_2O$ | 1.44 | 1.47 | 1.56 | 1.20 | 1.37 | 1.20 | 6.63 | .78 | 1.90 | .15 | 1.66 |
| $Na_2O$ | 2.15 | 2.73 | 2.90 | 2.84 | 2.44 | 2.21 | 3.50 | 1.24 | 4.74 | .10 | 4.96 |
| $P_2O_5$ | .40 | .42 | .42 | .59 | .57 | .58 | .01 | .02 | .03 | .00 | .10 |
| Loss | .01 | .01 | .01 | .01 | .01 | .00 | .02 | .01 | .01 | .01 | .01 |
| Total | 96.47 | 99.34 | 100.18 | 102.24 | 100.74 | 98.36 | 97.96 | 99.35 | 98.17 | 97.91 | 100.16 |
| FeO | 7.89 | 7.90 | 7.85 | 9.63 | 9.43 | 9.67 | - | - | - | - | - |
| $Fe_2O_3$ | 1.10 | 1.10 | 1.09 | 1.34 | 1.32 | 1.35 | - | - | - | - | - |
| Nb* | 22 | 23 | 20 | 16 | 23 | 22 | 0 | 0 | 2 | 0 | 0 |
| Zr* | 144 | 160 | 162 | 140 | 152 | 145 | 16 | 0 | 42 | 2 | 8 |
| Y* | 28 | 27 | 27 | 28 | 29 | 30 | 5 | 0 | 2 | 0 | 5 |
| Sr* | 354 | 330 | 339 | 367 | 366 | 371 | 146 | 116 | 341 | 17 | 496 |
| Rb* | 25 | 36 | 33 | 19 | 22 | 20 | 152 | 19 | 52 | 4 | 39 |
| Th* | 3 | 7 | 8 | 9 | 7 | 9 | 2 | 6 | 0 | 0 | 0 |
| Ni* | - | - | - | 113 | 114 | - | - | - | - | - | - |
| Cr* | - | - | - | 200 | 197 | - | - | - | - | - | - |
| Elev. | 400 | 400 | 100 | 100 | 200 | 100 | - | - | - | - | - |

*weight expressed in parts per million (ppm)

Appendix 2. Thermophysical properties of the average Ice Springs basalt.

DENSITY OF EQUIVALENT LIQ. DRY AND AT 500. BARS P H2O

| T DEG C | 700. | 800. | 900. | 1000. | 1100. | 1200. | 1300. | 1400. | 1500. |
|---|---|---|---|---|---|---|---|---|---|
| DEN WET | 2.703 | 2.688 | 2.672 | 2.656 | 2.641 | 2.625 | 2.609 | 2.593 | 2.578 |
| DEN DRY | 2.731 | 2.716 | 2.701 | 2.686 | 2.671 | 2.656 | 2.641 | 2.626 | 2.611 |

DENSITY (WET) = -.000157 T + 2.8134 (T DEG C)
DENSITY (DRY) = -.000151 T + 2.8366 (T DEG C)

HEAT CAPACITY OF SILICATE LIQUID
CP = 21.09 (CAL/MOLE-DEG)
CP = .34 (CAL/GRAM-DEG)

GRAM FORMULA WEIGHT
ANHYDROUS = 61.33
HYDROUS = 60.70

LOGARITHM (10) OF VISCOSITY OF LIQUID (POISE)

| T DEG C | 700. | 800. | 900. | 1000. | 1100. | 1200. | 1300. | 1400. | 1500. |
|---|---|---|---|---|---|---|---|---|---|
| DRY | 6.18 | 5.20 | 4.39 | 3.70 | 3.12 | 2.62 | 2.18 | 1.79 | 1.44 |
| WET | 5.93 | 4.98 | 4.19 | 3.52 | 2.96 | 2.47 | 2.04 | 1.66 | 1.33 |

LN VISCOSITY (DRY) = 23496.23/T DEG K -9.9244
LN VISCOSITY (WET) = 22842.89/T DEG K -9.8264

THERMAL CONDUCTIVITY OF EQUIVALENT LIQUID (X $10^{-3}$)

| T DEG C | 700. | 800. | 900. | 1000. | 1100. | 1200. | 1300. | 1400. | 1500. |
|---|---|---|---|---|---|---|---|---|---|
| | .91 | 1.17 | 1.48 | 1.86 | 2.30 | 2.81 | 3.40 | 4.07 | 4.83 |

THERMAL CONDUCTIVITY + .85-12 $T^3$ + .12/T (CAL/CM-SEC-DEG K)

THERMAL DIFFUSIVITY OF LIQUID (X $10^{-3}$) ($CM^2$/SEC)

| T DEG C | 700. | 800. | 900. | 1000. | 1100. | 1200. | 1300. | 1400. | 1500. |
|---|---|---|---|---|---|---|---|---|---|
| | .97 | 1.25 | 1.60 | 2.01 | 2.50 | 3.08 | 3.74 | 4.51 | 5.38 |

KINEMATIC VISCOSITY (STOKES) ($CM^2$/SEC)

| T DEG C | 700. | 800. | 900. | 1000. | 1100. | 1200. | 1300. | 1400. | 1500. |
|---|---|---|---|---|---|---|---|---|---|
| DRY | .55+06 | .58+05 | .90+04 | .19+04 | .49+03 | .16+03 | .57+02 | .23+02 | .11+02 |

COEFFICIENT OF THERMAL EXPANSION OF LIQUID (X 10 TO THE -4) (/DEG)

| T DEG C | 700. | 800. | 900. | 1000. | 1100. | 1200. | 1300. | 1400. | 1500. |
|---|---|---|---|---|---|---|---|---|---|
| | .5992 | .5957 | .5921 | .5886 | .5852 | .5818 | .5784 | .5751 | .5718 |

Appendix 3. Formula for calculation of effective Rayleigh numbers.

$$R_a \text{ (effective)} = R_a \text{ (thermal)} - R_a \text{ (solutal)}$$

$$= gB\,(T_o - T_1)d^3 / vk - gd^4(X_o - X_1) / LvD_{ab}$$

$$= gB\,(\Delta T)d^3 / vk - gd^4(\Delta X) / LvD_{ab}$$

where:

g = gravitational constant = 980 $cm/sec^2$
B = coefficient of thermal expansion = $(1/V_o)dV/dT$
d = diameter of chamber
L = length of chamber
v = kinematic viscosity
k = thermal conductivity
$X_i$ = mole fraction of component i at boundary
$T_i$ = temperature of system at boundary
$D_{ab}$ = diffusivity of component a in b.
$\varsigma$ = $(1/p_o)dp/\Delta X$

For the Ice Springs magma system the following average values were used with various chamber configurations and thermal differences: (T = 1000°C)

B = $5.886 \times 10^{-3}$ /deg
v = $.19 \times 10^4 cm^2/sec$
k = $1.86 \times 10^{-3}$
D = $10^{-5}$(approximate value for general diffusivity of system)
$p_o$ = 2.686(dry)

## REFERENCES


Bowen, N. L., 1928, The evolution of igneous rocks: Princeton University Press, Princeton, New Jersey.

Brownlee, K. A., 1965, Statistical theory and methodology in science and engineering: John Wiley and Son, New York.

Buddington, A. F., and Lindsley, D. H., 1964, Iron-titanium oxide minerals and synthetic equivalents: Jour. Petrol., v. 5, p. 310-351.

Carrier, D. L., 1979, Gravity and heat flow studies at Twin Peaks: an area of late Tertiary silicic volcanism in Millard County, Utah: unpubl. M. S. Thesis, University of Utah, 119 p.

Chen, C-H., and Presnall, D. C., 1975, The system $Mg_2SiO_4$-$SiO_2$ at pressures up to 25 kilobars: Amer. Min. v. 60, p. 398-406.

Clark, E. E., 1974, Late Cenozoic volcanic and tectonic activity along the eastern margin of the Great Basin, in the proximity of Cove Fort, Utah: Brigham Young Univ., Geol. Studies, v. 24, p. 87-114.

Condie, K., and Barsky, C., 1972, Origin of Quaternary basalts from the Black Rock Desert region, Utah: Geol. Soc. Amer. Bull., v. 28, p. 333-352.

Dalrymple, G. B., 1969, 40Ar/35Ar analyses of historic lava flows: Earth Planet. Sci. Letters 6, p. 47-55.

Davis, J. C., 1973, Statistics and data analysis in geology: John Wiley and Sons, New York.

Deer, W. A., Howie, R. A., and Zussman, J., 1977, Rock forming minerals: Volume 2A Single Chain Silicates, John Wiley and Sons, New York.

Donaldson, C. H., Usselman, T. M., Williams, R. J., and Lofgren, G. E., 1975, Experimental modeling of the cooling history of Apollo 12 olivine basalts: Proc. Lunar Sci. Conf. 6th, p. 843-869.

Evans, S. H., and Nash, W. P., 1979, Petrogenesis of xenolith bearing basalts from southeastern Arizona: Amer. Mineral., v. 64, p. 249-267.

Faure, G., 1977, Principles of Isotope Geology: John Wiley and Sons, New York.

Flanagan, 1972, F. J., 1972, 1972 values for international geochemical reference samples: Geochim. et Cosmochim. Acta, v. 37, p. 1189-1200.

Frey, F. A., Green, D. H., and Roy, S. D., 1977, Integrated models of basalt petrogenesis: a study of quartz tholeiites to olivine melilities from south eastern Australia utilizing geochemical and experimental petrological data: Jour. Petrol., v. 19, no. 3, p. 463-513.

Frey, F. A., 1979, Trace element geochemistry: Applications to the igneous petrogenesis of igneous rocks: Review Geophy. Space Physics, v. 17, no. 4, p. 803-823.

Gast, R. W., 1968, Trace element fractionation and the origin of tholeiitic and alkaline magma types: Geochim. et Cosmochim. Acta, v. 32, p. 221-235.

Gilbert, G. K., 1890, Lake Bonneville: U. S. Geol. Surv. Monograph 1, p. 319-339.

Hedge, C. E., and Stacey, J. S., 1980, Precambrian geochronology of northern Utah: Abstracts with Programs, Rocky Mountain Section Geol. Soc. Amer., v. 12, no. 6, p. 275.

Hoover, J. D., 1974, Periodic Quaternary volcanism in the Black Rock Desert, Utah: Brigham Young Univ., Geol. Studies, v. 21, p. 2-72.

Irvine, T. N., 1979, Rocks whose composition is determined by crystal accumulation and sorting In H. S. Yoder, Ed. The Evolution of Igneous Rocks: Fiftieth Anniversary Perspectives: Princeton University Press, Princeton, New Jersey.

Irving, A. J., 1978, A review of experimental studies of crystal/liquid trace element partitioning: Geochim. et Cosmoschim. Acta, v. 42, p. 743-770.

Leeman, W. P., 1976, Petrogenesis of McKinney (Snake River) olivine tholeiite in light of rare-earth and Cr/Ni distributions: Geol. Soc. Amer. Bull., v. 87, p. 1582-1586.

Nash, W. P., and Crecraft, H., 1979, Petrology and geochronology of late Tertiary and Quaternary volcanic rocks in the eastern margin of the Basin and Range Province, Utah: Final report, v. 3, U.S. Geol. Surv. Contract 14-08-0001-G-343, Dept. Geol. and Geophysics, University of Utah.

Norrish, K., and Hutton, J. T., 1969, An accurate X-ray spectrographic method for the analysis of a wide range of geological samples: Geochim. et Cosmochim. Acta, v. 33, p. 431-453.

Olson, T. L., and Smith, R. B., 1976, Earthquake survey of the Roosevelt Hot Springs and Cove Fort areas, Utah: NSF Final Report, v. 4, University of Utah Contract GI-43741.

Powell, M., and Powell, R., 1974, An olivine-clinopyroxene geothermometer: Contrib. Mineral. Petrol., v. 48, 249-263.

Puskar, C., and Condie, K. C., 1973, Origin of the Quaternary basalts from the Black Rock Desert, Utah: Strontium-isotopic evidence: Geol. Soc. Amer. Bull., v. 84, p. 1053-1058.

Roeder, P. L., and Emslie, R. F., 1970, Olivine-liquid equilibrium: Contr. Mineral. Petrol., v. 29, p. 275-289.

Selk, D. C., 1976, Crustal and upper mantle structures in Utah as determined by gravity profiles: unpubl. M. S. Thesis, Univ. of Utah.

Serpa, L. F., and Cook, K. L., 1980, Detailed gravity and aeromagnetic surveys in the Black Rock Desert area, Utah: Topical report IDO/DOE/ET28392/39, 78-1701.a.5.3.

Shaw, D. M., 1970, Trace element fractionation during anatexis: Geochim. et Cosmochim. Acta, v. 34, p. 331-340.

Stormer, J. C., Jr., and Nicholls, J., 1978, XLFRAC: A program for the interactive testing of magmatic differentiation models: Computers and Geosciences, v. 4, p. 143-159.

Taylor, H. P., Jr., Giannetti, B., and Turi, B., 1980, Oxygen isotope geochemistry of the Potassic igneous rocks from the Roccamonfina volcano, Roman Comagmatic Region, Italy: Contin. no. 3142, Div. Geol. Planet. Sciences, Calif. Inst. Tech., Paseadena, Calif.

Turner, J. S., 1973, Buoyancy effects in fluids: Cambridge Monographs on mechanics and applied mathematics: Cambridge University Press, Cambridge.

Valastro, S., Jr., Davis, E. M., and Varela, A. G., 1972, University of Texas at Austin Radiocarbon dates IX: Radiocarbon, v. 14, p. 461-485.

Vance, J. A., 1969, On Synneusis: Contrib. Mineral. Petrol., v. 24, p. 7-29.

Wilcox, R. E., 1979, The liquid line of descent and variation diagrams In H. S. Yoder, Ed., The Evolution of Igneous Rocks: Fiftieth Anniversary Perspectives: Princeton University Press, Princeton, New Jersey.

Williams, H. and McBirney, A. R., 1979, Volcanology: Freeman, Cooper,

and Co., San Francisco.

Wood, B. J., and Banno, S., 1973, Garnet-orthopyroxene and orthpyroxene-clinopyroxene relationships in simple and complex systems: Contrib. Mineral. Petrol., v. 42, p. 109-124.